SANDIA REPORT
SAND2002-1466
Unlimited Release
Printed May, 2002

Microstructures, Phase Formation, and Stress of Reactively-Deposited Metal Hydride Thin films

David P. Adams, Juan A. Romero, Mark A. Rodriguez, Jerry A. Floro, and Paul G. Kotula

Prepared by
Sandia National Laboratories
Albuquerque, New Mexico 87185 and Livermore, California 94550

Sandia is a multiprogram laboratory operated by Sandia Corporation, a Lockheed Martin Company, for the United States Department of Energy under Contract DE-AC04-94AL85000.

Issued by Sandia National Laboratories, operated for the United States Department of Energy by Sandia Corporation.

Available to DOE and DOE contractors from
U.S. Department of Energy
Office of Scientific and Technical Information
P.O. Box 62
Oak Ridge, TN 37831

Telephone: (865)576-8401
Facsimile: (865)576-5728
E-Mail: reports@adonis.osti.gov
Online ordering: http://www.doe.gov/bridge

Available to the public from
U.S. Department of Commerce
National Technical Information Service
5285 Port Royal Rd
Springfield, VA 22161

Telephone: (800)553-6847
Facsimile: (703)605-6900
E-Mail: orders@ntis.fedworld.gov
Online order: http://www.ntis.gov/ordering.htm

SAND2002-1466
Unlimited Release
Printed May 2002

Microstructure, Phase Formation, and Stress of Reactively-Deposited Metal Hydride Thin Films

David P. Adams, Juan A. Romero, Mark A. Rodriguez≠,

Jerry A. Floro#, and Paul G. Kotula≠

Thin Film, Vacuum and Packaging Department
≠ Materials Characterization Department
Surface and Interface Science Department
Sandia National Laboratories
P.O. Box 5800
Albuquerque, NM, 87185-0959

Abstract

This document summarizes research of reactively deposited metal hydride thin films and their properties. Reactive deposition processes are of interest, because desired stoichiometric phases are created in a one-step process. In general, this allows for better control of film stress compared with two-step processes that react hydrogen with pre-deposited metal films. Films grown by reactive methods potentially have improved mechanical integrity, performance and aging characteristics.

The two reactive deposition techniques described in this report are reactive sputter deposition and reactive deposition involving electron-beam evaporation. Erbium hydride thin films are the main focus of this work. ErH_x films are grown by ion beam sputtering erbium in the presence of hydrogen. Substrates include αAl_2O_3 {0001}, αAl_2O_3 {11$\underline{2}$0}, Si{001} having a native oxide, and polycrystalline molybdenum substrates. Scandium dideuteride films are also studied. ScD_x is grown by evaporating scandium in the presence of molecular deuterium. Substrates used for scandium deuteride growth include single crystal sapphire and molybdenum-alumina cermet. Ultra-high vacuum methods are employed in all experiments to ensure the growth of high purity films, because both erbium and scandium have a strong affinity for oxygen.

Film microstructure, phase, composition and stress are evaluated using a number of thin film and surface analytical techniques. In particular, we present evidence for a new erbium hydride phase, cubic erbium trihydride. This phase develops in films having a large in-plane compressive stress independent of substrate material. Erbium hydride thin films form with a strong <111> out-of-plane texture on all substrate materials. A moderate in-plane texture is also

found; this crystallographic alignment forms as a result of the substrate/target geometry and not epitaxy. Multi-beam optical sensors (MOSS) are used for in-situ analysis of erbium hydride and scandium hydride film stress. These instruments probe the evolution of film stress during all stages of deposition and cooldown. Erbium hydride thin film stress is investigated for different growth conditions including temperature and sputter gas, and properties such as thermal expansion coefficient are measured. The in-situ stress measurement technique is further developed to make it suitable for manufacturing systems. New features added to this technique include the ability to monitor multiple substrates during a single deposition and a rapidly switched, tiltable mirror that accounts for small differences in sample alignment on a platen.

ACKNOWLEDGMENTS

The authors appreciate the efforts of R.W. Buttry (for Auger Electron Spectroscopy), J. Hunter (for help with MOSS), J. Banks (for ion beam analysis), R. Goeke (for ScD_2 experiments), T. Buchheit (help with tensor calculations), S. van Deusen (for ion beam analysis), N. Moody (for nanoindentation), and L. Brown with D. van Ornham (for cermet substrate fabrication). Discussions with E. Chason, L. Beavis, B. Doyle were informative and useful. The improvements to the multi-beam stress sensor were completed with k-Space Associates, Inc. This work was performed at Sandia National Laboratories and is supported by the United States Department of Energy under Contract No. DE-AC04-94AL85000. Sandia is a multiprogram laboratory operated by Sandia Corporation, a Lockheed Martin Company, for the United States Department of Energy.

This work was supported through LDRD programs and the Advanced Manufacturing Investment area.

Contents

Section I. Interest in metal hydride thin films and reactive deposition techniques…..…. 7

Section II: Crystal structures of erbium and scandium hydrides ……...…. 10

Section III: Background: Thin film stress and techniques for measuring this property. 12

Section IV: Reactive ion beam sputtered erbium hydride……...…. 14

Section V: Reactive deposition of scandium deuteride……...… 41

REFERENCES …….….. 49

APPENDIX 1 ……..… 51

APPENDIX 2 ……..… 53

APPENDIX 3 ……..……...… 54

APPENDIX 4 ……..…….. 55

APPENDIX 5 ……..…….. 56

APPENDIX 6…… 57

Section I. ***Interest in metal hydride thin films and reactive deposition techniques***

Metal hydride thin films are of interest for a variety of applications including defense programs, fuel cells, down-hole oil-logging devices, and neutron sources for medical imaging and diagnostics. In addition, certain metal hydride thin films have recently attracted attention, for these materials exhibit interesting optical and magnetic properties. Extensive work by Griessen et. al.[1-3] and others[4] investigates the growth of yttrium and lanthanum hydrides, while demonstrating feasibility as switchable mirrors. Additional research investigates the effects of hydrogen loading on film structure and phase formation.[5-8]

In previous work, including that by Griessen, vapor deposited metal hydride thin films are fabricated by two-step processes involving evaporation of metal and subsequent hydrogen loading. In some cases hydrogen is loaded through a Pd overlayer after removal from the thin film deposition system.

Two-step processes, however, are characterized by large stress that approaches the yield point of the material. High stress often accompanies hydriding and cooldown from the growth temperature. In recent work, the evolution of ScD_2 film stress is investigated for films grown by two-step processes.[9] Thin films are fabricated by depositing Sc via evaporation, followed by high temperature loading of deuterium at the growth temperature. Typical changes in stress that accompany thin film fabrication are indicated in Figures 1 and 2 for different substrate materials. As shown in both figures, Sc metal thin films have a relatively low stress at the growth temperature (step 2). However, reaction of scandium metal with deuterium at elevated temperature to form a stoichiometric dideuteride phase leads to a large compressive in-plane film stress. Compression during hydriding results from an increased atomic density compared with the as-deposited metal film. After reaction with deuterium, samples are cooled to

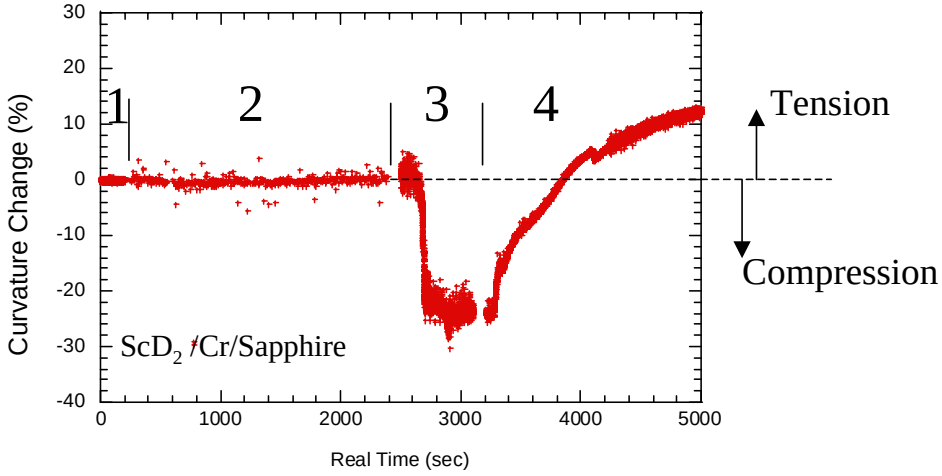

Figure 1. *taken from reference 9*. Changes in sapphire wafer curvature during thin film fabrication . Minimal stress changes are observed during Sc metal deposition (step 2). Films develop compressive stress during reaction with D_2 (step 3) and a tensile stress during cooldown (step 4).

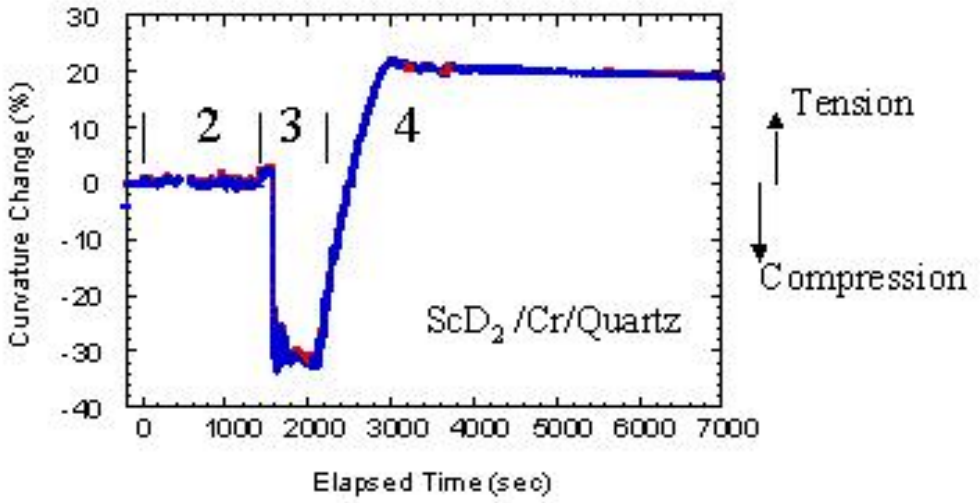

Figure 2. *taken from reference 9* Changes in quartz wafer curvature during processing of ScD_2 / Cr thin films. Step 2 corresponds to metal deposition, step 3 is hydriding and step 4 involves cooldown to ambient temperature. The sudden change in slope during step 4 results from stress relief via cracking.

ambient temperature, and a tensile stress develops due to mismatched coefficients of thermal expansion (CTE) of the substrate-film couple. The residual film stress and the propensity for films to crack during cooldown depends on the substrate material when using identical process parameters. Films deposited onto quartz substrates show evidence of stress relief during cooldown (time = 3000 sec) due to a large CTE misfit; this is correlated with crack nucleation and propagation within films. On the other hand, no cracks are observed when deposited onto sapphire substrates. [9]

Alternative growth techniques that allow control of metal hydride thin film stress are desired, because these may improve long-term reliability and performance. In general, the stress of an as-deposited film is considered critical to its mechanical integrity. Although a few applications benefit from a controlled, low amount of strain, excessive stress most often compromises adhesion to a substrate. Films may plastically yield due to significant stress, but, in many cases, coatings detach from a wafer due to insufficient interfacial toughness. Stress is a material property that can, if uncontrolled, lead to the immediate rejection of an entire production lot.

Furthermore, changes in film stress can occur over time by aging. This includes the individual or cumulative effects of radioactive decay, outgassing, absorption, repeated operation/testing at high temperature and other effects. Tailoring the initial stress state of a film may extend its useful life and, thus, improve performance. If known changes in stress occur over time for a given material system, it is anticipated that tailoring a film's initial properties can compensate these effects.

Finally, stress, in certain circumstances, can be exploited for tailoring film structure. Residual stress is known to affect the stability of crystal structures for some

material systems. Cubic boron nitride is a well-known example of a high-pressure phase that can be stabilized when it is formed as a high-stress thin film.

In the current study, we research deposition techniques that allow control of film stress. This includes reactive deposition techniques that simultaneously expose the surface of a growing film to vapors of all intended species. This is advantageous compared with other techniques, because desired phases can be formed layer by layer. By bringing all required atomic species to the growth surface throughout the deposition, there is an excellent chance to remove potentially compromising high stress and to establish a film having a zero average stress. For current work, metal and hydrogen are co-deposited with the goal of forming stoichiometric metal hydrides.

We include study of reactive sputter deposition, because this technique should provide greater flexibility in tailoring stress state (compressive, zero or tensile) compared with alternative processes such as evaporation and chemical vapor deposition. Secondly, sputter deposition offers the ability to lock in a particular stress magnitude. It is known from previous research of reactively deposited nitrides and oxides that a film having a particular tensile, compressive, or near-zero stress can be deposited. In some cases, the stress in sputtered films can be controlled at a near-zero magnitude or to levels as high as several hundred MPa or a few GPa (one GPa equates to 10^4 atmospheres internal pressure). When using sputter deposition, the magnitude of the stress can be controlled by changing one or more process parameters. For example, sputter pressure can be used to manipulate stress. An example of this is shown in Figure 3 for magnetron sputtered Er films on Si(100) for fixed growth temperature (T_g) of 30^{o}C.

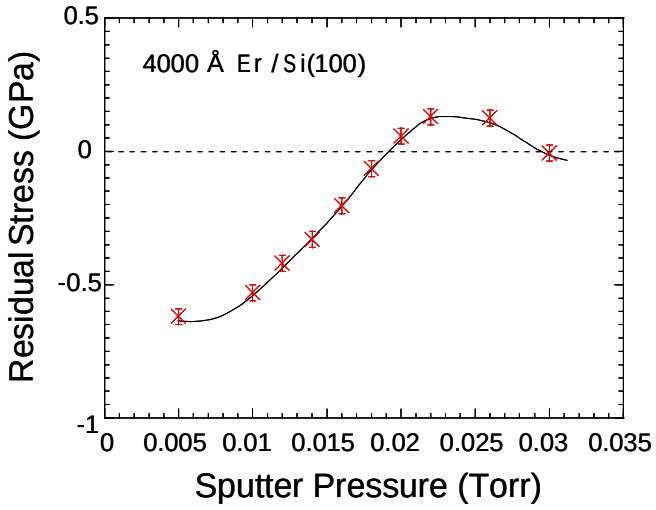

Figure 3. Plot of residual stress for Er/Si(100) as determined by a Flexus Tencor laser scanning device. The silicon substrate has a native oxide. T_g =30^{o}C.

As part of our research, the crystal phase and microstructure are researched thoroughly, for these are expected to be different than those formed using alternative

growth techniques. Various thermodynamic and kinetic factors can affect structure and morphology; these factors are specific to each growth technique. Other differences in sputtered versus evaporated film composition and structure may also affect aging. The presence of inert sputter gas atoms trapped in films may be relevant.

Section II: *Crystal structures of erbium and scandium hydrides*

For this research, we focus on two metal hydride thin film systems. This includes erbium hydride and scandium hydride.

Below is a description of known crystallographic structures for these two material systems. While subtle differences in lattice spacings develop for different hydrogen isotopes, it is emphasized that the same crystal lattice types form with protium, deuterium and tritium. We also show their phase diagrams, taken from previous reports. The structures and phases reported in this section represent the state of knowledge prior to our research.

Er-H system

The erbium - hydrogen system has been studied in the past by various crystallographic analysis techniques. This includes investigations of erbium hydride thin films grown on various substrates and bulk specimens.[10,11] Two well-characterized erbium hydride phases, having different crystal lattice structures, are identified in these studies. Similar to Tb, Dy, Ho, Y, Lu and Tm, erbium forms a cubic dihydride phase and a hexagonal trihydride phase.[12] The thermodynamically-stable ErH_2 structure is that of fluorite (CaF_2). A drawing of this cubic phase is shown in Figure 4. ErH_3 is shown to have a 'HoH_3 type structure' with a space group P3cl (D^4_{3d}).[13] This can be envisioned as a hexagonal close-packed metal lattice with H atoms situated in positions that are slightly displaced from the tetrahedral and octahedral interstitial sites. An erbium – hydrogen phase diagram[14] is shown in Figure 5.

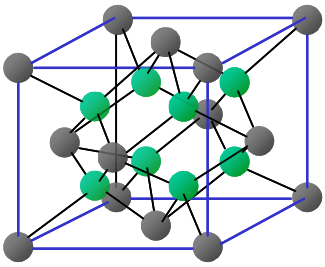

Figure 4. Fluorite structure of cubic ErH_2. The face centered cubic sublattice shows the positions of Er atoms. H is located at the <1/4,1/4,1/4> sites.

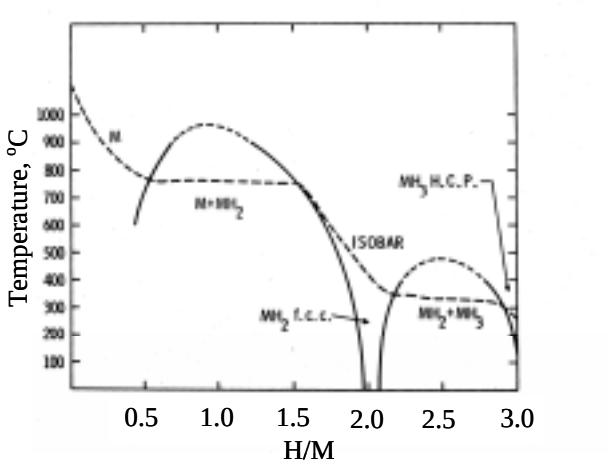

Figure 5. Erbium – hydrogen phase diagram from L. Beavis (1968), reference 14.

Sc-H system

For a complete discussion of the scandium – hydrogen system and its crystal phases (including those formed at high pressure), we suggest reading of a paper by Manchester and Pitre.[15] In that publication, the authors summarize previous work and their own to generate a T-χ phase diagram for P < 0.13 MPa. This is shown in Figure 6. Current understanding of this material system indicates that a ScH_x phase, labeled here as δ, has the fluorite structure over a broad range of temperatures. This is the same structure in almost all Ln - H systems in the x~2 concentration range. According to the authors, the (αSc+ δ / δ) boundary at room temperature is located at x=1.68 (62.7%H). This is a considerably lower x than for other Ln-H – type systems (e.g., La-H, Ce-H and Sm-H). Of less relevance to our report, another interesting feature is found on the low concentration side of this phase diagram. An unusually large α–metal phase field is shown maintained to low temperatures. The (αSc/ αSc + δ) phase boundary extends to x = 0.4 at room temperature. The αSc phase is considered a random interstitial alloy of H in the hexagonal lattice of Sc. The H is known to occupy tetrahedral sites of the metal sublattice.[16] Unlike the Er - H system there is no hexagonal trihydride phase *at moderate pressures*. Evidence for a high-pressure scandium trihydride phase is discussed in reference 15.

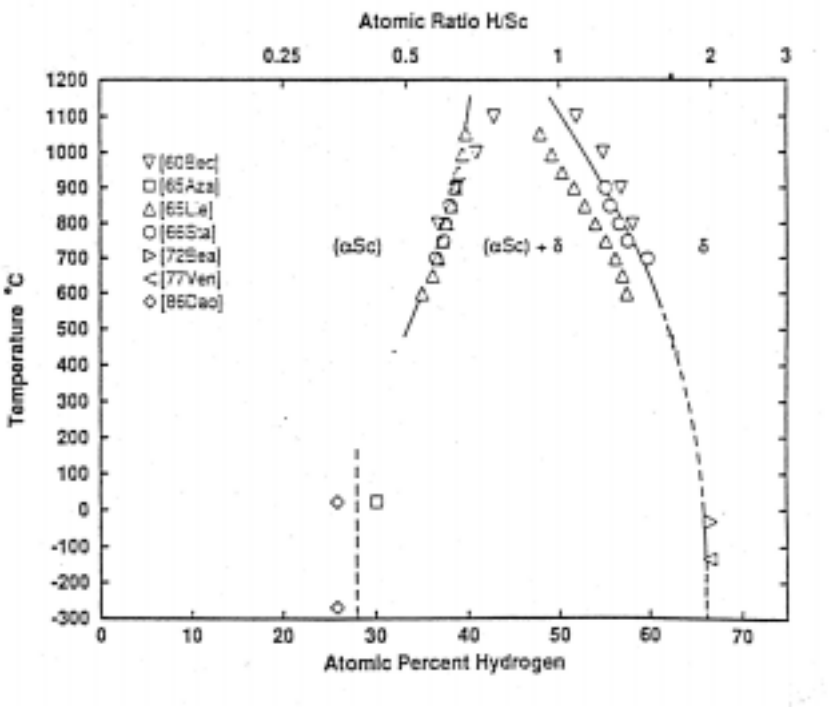

Figure 6. Sc-H phase diagram from Manchester and Pitre (1997).

Section III*: Background: Thin film stress and techniques for measuring this property*

Thin film stress developed during processing is often distinguished in terms of intrinsic and extrinsic effects. Intrinsic stress is related to the density and microstructure of a layer. It can develop due to changes in the number of point, line and planar defects per unit volume, grain structure, phase and lattice type. Because microstructure depends sensitively on the process (source/substrate geometry, growth temperature and deposition rate), intrinsic stress is directly affected by the growth parameters. Extrinsic stress, on the other hand, develops from the thermomechanical behavior of a thin film-substrate couple. Often thin films are deposited at high temperature and then cooled prior to removal from a vacuum system. If a film and substrate are dissimilar materials, a change in temperature can generate significant extrinsic stress due to mismatched coefficients of thermal expansion. Note, generation of extrinsic stress can also occur during high temperature operation of a thin film. Applications that require high temperature excursions or isothermal anneals are subject to changes in stress, and, once cooled, films may return to a stress state different than that prior to heating.

As indicated in Figures 1 and 2, two nonzero stress 'types' characterize thin films. This includes compressive and tensile stress. Both types of stress can develop during film fabrication or operation, and each may degrade the mechanical stability of a coating. It is well-known that stress causes a number of structural or morphological changes. If sufficiently large, compressive stress leads to film decohesion. This is characterized by blisters or buckles (sometimes cracked) that extend across a wafer. Large tensile stress generates cracks, and fracture may occur within a film or a substrate. If uncontrolled, both types of stress lead to complete spallation.

In current work, we desire to study the evolution of stress during reactive deposition. We therefore require an *in-situ* probe of film stress that monitors the properties of an evolving film contained within the vacuum apparatus. This instrument must noninvasively 'peer' into the chamber and relay details about a film to the operator. Analysis must not affect the growth process by heating substrates or inducing undesired chemical reactions. The analytical technique must, however, be sensitive, since changes in stress can rapidly occur over seconds. For manufacturing, *in-situ* monitoring techniques provide the opportunity for real-time process control of film stress.

A number of analytical techniques are capable of probing thin film stress *in-situ*. For example, diffraction-based techniques including conventional x-ray diffraction, grazing incidence x-ray scattering, and reflection high-energy electron diffraction are commonly used in research laboratories. These techniques are used to determine strain by measuring the deviation of a film's lattice parameters from known equilibrium values. For the purpose of investigating metal hydride thin film processes, particularly those involving sample rotation, diffraction-based techniques are considered difficult. Although these techniques are sensitive, the precise geometry required for analysis is difficult to maintain, particularly with moving samples. We envision that an unwieldy 'stop and go' procedure would be required for thin film analysis when using these techniques.

Instead, an *in-situ* wafer curvature measurement technique is chosen. Wafer curvature techniques[17] are attractive for determining thin film stress in a manufacturing setting with moving samples. In general, a number of methods have been devised including x-ray techniques (double crystal diffraction topography)[18] and a variety of laser-based diagnostics that operate at visible wavelengths. Each of these probe substrate shape before and after thin film growth, and stress can be calculated from measured curvature changes if certain conditions are maintained. Laser-based instruments are preferred, because they are noninvasive, sensitive and simpler to operate than x-ray techniques. Typically light enters through a viewport, strikes a sample and returns to a camera for analysis. The radiant power impinging on a sample is a few microWatts, insufficient to cause significant heating. In most cases, the entire laser apparatus is maintained external to the vacuum. Only a clear viewport and a direct line to a sample is required. Several forms of laser-based, light scattering instruments have been investigated previously. This includes laser scanners which steer a beam of light across a wafer to determine curvature. This has high sensitivity for benchtop experiments, but is considered unsuitable for growth processes involving moving substrates.

For the present work, a multi-beam, optical stress sensor, referred to as MOSS, is chosen. This technique was originally developed by E. Chason, J.A. Floro et. al. at Sandia National Laboratories[19] and commercialized by k-Space Associates, Inc. (Ann Arbor, MI). The technique involves directing an array of laser light spots onto a substrate in order to accurately map curvature. Stress is determined via Stoney's[20] or other formulations. The MOSS technique is an improvement over other optical-based techniques, because it simultaneously illuminates a substrate with an array of beams. Multiple beams of light are reflected from a sample without the need for mechanical raster, thus allowing rapid detection. The technique also allows for a sensitive measurement of stress, because noise introduced from vibrating pumps, heaters, etc. is reduced. Analysis involves the determination of reflected laser spot centroid positions, and spot spacings are used to quantify curvature. Because the array is most often deflected uniformly as a result of vibration, the more important spot spacings that determine curvature remain largely unaffected. Sensitive measurements of stress have been conducted on a number of thin film systems using the MOSS technique. This includes measurement of stress in layers as thin as 0.1 monolayers (Ge on a Si(001)).[21] Recent work by Hearne et. al.[22] probes stress during deposition and temperature cycling.

Section IV: ***Reactive ion beam sputtered erbium hydride***

This section describes the initial results of depositing erbium hydride reactively. Reactive sputter deposition is researched as a method for depositing erbium hydride thin films, because, in general, this technique provides better control of residual stress. For current work we employ ion beam sputtering as a method for growth. It is recognized at the onset of this research that ion beam sputter deposition is likely to produce compressively stressed coatings or near-zero stress films. Future work investigates additional sputter deposition techniques that allow even greater flexibility in tailoring stress.

A challenge of this research is to control stress in metal hydrides while maintaining required stoichiometries (hydrogen/metal ratio). The growth of erbium hydride by sputtering is also challenging, because this growth technique is considered less pure compared with evaporative deposition. Er has a strong affinity for oxygen, and methods to reduce oxygen levels in films are vital to success.

Metal hydride sputter deposition and analysis system

A sputter deposition system is custom-built for researching the growth of high-purity erbium hydride thin films and the evolution of stress in these coatings. This apparatus is cryopumped and has a base pressure of 1 x 10^{-9} Torr (after bakeout), as indicated by a stable ion gauge. A static deposition geometry is employed for film growth. For all deposition experiments, samples are fixed 23 cm from the surface of a 10 cm-diameter, high purity (99.95%) Er sputter target. The substrate normal direction is fixed in all experiments and is not aligned with the target normal as shown in Figure 7.

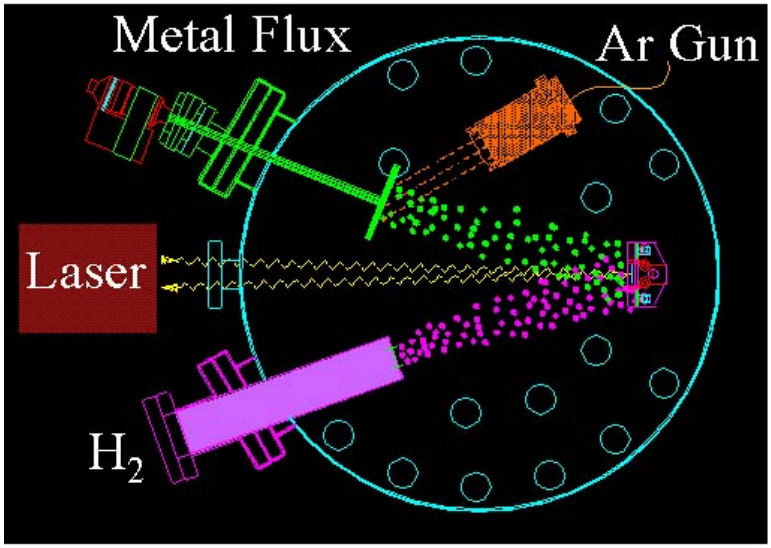

Figure 7. Chamber schematic showing Kaufmann sputter gun and sputter target / sample geometry. Also shown is the position of the laser used for *in-situ* monitoring of stress.

A Kaufmann ion source (Commonwealth Scientific) is used for inert gas sputtering of erbium. The ion source is oriented so that gas ions impinge at a 48^{o} incidence angle relative to target normal. Ion beam sputtering is used despite its relatively slow rate of deposition; this allows for front-side viewing access of the sample and for *in-situ* measurements of stress using MOSS. For the majority of experiments, ultra-high purity (99.999%) or research grade Ar is used for sputtering, with the pressure regulated by a mass flow controller. A getter filter is used to maintain high purity sputter gas. The Ar partial pressure used for these experiments is 6.6×10^{-4} Torr. Ultra-high purity (99.999%) H_2 is passed through a second getter filter (SAES), and a separate mass flow controller prior to entering the chamber. Hydrogen is introduced into the chamber in one of two ways. A few experiments use an electron cyclotron resonance (ECR) plasma source (Astex) to generate a beam of pure hydrogen (arriving in the form of mixed H_2^+, H and H^+). The hydrogen species are directed at the sample during growth as shown in Figure 7. Because an ECR source operates at microwave frequencies it does not require a carrier gas and maintains high purity. The majority of reactive sputter depositions involve backfilling the chamber with molecular hydrogen to a partial pressure of 1.4×10^{-4} Torr. For these experiments the ECR source is removed from the deposition system, and hydrogen is introduced through a separate line having the same mass flow controller and getter filter. It is understood that the erbium target absorbs a significant amount of hydrogen during deposition, and hydrogen may arrive at the film growth surface in forms other than H_2. Er is sputtered in the presence of flowing H_2 for many minutes prior to each deposition in order to equilibrate the near surface region of the target and to establish a constant deposition rate.

A sample holder with heating stage and backside thermocouple is custom built for this research project, as shown in Figure 8. It provides heating to temperatures as high as $\sim 550^{o}$C using a backside, noncontact boralectric heater. A stainless steel cage is built around the holder assembly for uniform heating; a window is machined in the front to allow for deposition. Control experiments show that operation of the sputter gun generates a minimal amount of excess heat on the sample. This is compensated well by computer feedback control of the boralectric heater current. One sample is typically loaded into the chamber for an experiment; although, as many as two rectangular samples can be held vertically by separate Mo inserts. Each Mo holder clamps one side of a rectangular substrate in a springboard configuration. A second sample is clamped into position only for precise determination of the growth temperature. For the few experiments requiring a second sample, we contact the substrate directly with a thermocouple but avoid contact with the first sample so to maintain a geometry appropriate for curvature measurements. Silicon sample temperature is also calibrated using an optical pyrometer. The window on the front side of the cage also allows access of the polished substrate and film for pyrometry and laser curvature measurements. The entire holder assembly can be tilted slightly to align to the MOSS laser beams.

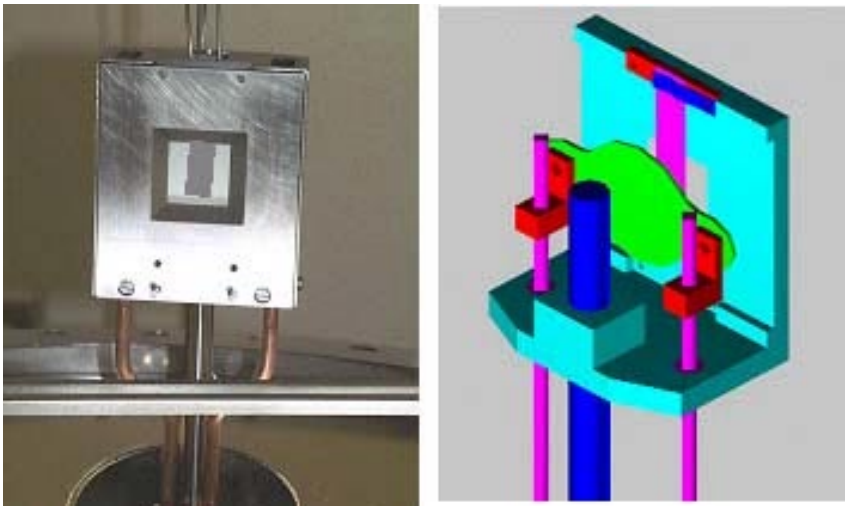

Figure 8. Substrate holder/heater built for ion beam sputter deposition system. Drawing on right does not show cover and thermocouple. This is designed to hold one or two rectangular substrates vertically.

The *in-situ* laser stress sensor used for erbium hydride thin film deposition experiments is shown below in Figure 9. It includes a laser, optics, mirrors and a high resolution CCD camera. We use a Melles Griot 56 InGaAlAs laser (λ = 658 nm) and a focusing lens in conjunction with two etalons to generate a two-dimensional array of parallel laser beams. The two-dimensional array of laser beams is incident on the film side of fixed substrates. New features added to this instrument include a rapidly switched, tiltable mirror. Although this can be used during thin film fabrication to account for small changes in sample tilt (e.g., those experienced during cooldown), we only use it prior to deposition to direct reflected laser spots onto the CCD camera. The mirror is useful for locating the reflected laser spots without opening the laser cover. In addition, real-time, computer control of laser output power maintains a near-constant reflected laser spot power on the CCD camera during erbium hydride depositions. This feature is essential for measurements of curvature taken from the film-growth side of a substrate, since changes in reflectivity (resulting from film growth) can modify the reflected laser light intensity. The camera has a 768 x 493 pixel detector, and it can operate at high speeds (e.g., shutter opening times as small as 1/10,000 sec). Control of shutter speed does not seem to improve the sensitivity of detection (by reducing noise), but it provides flexibility for working with samples of different reflectivity.

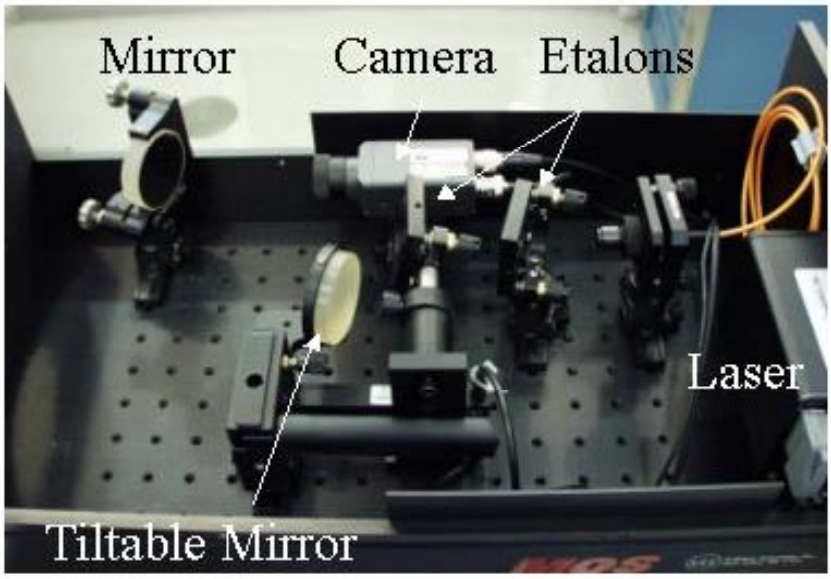

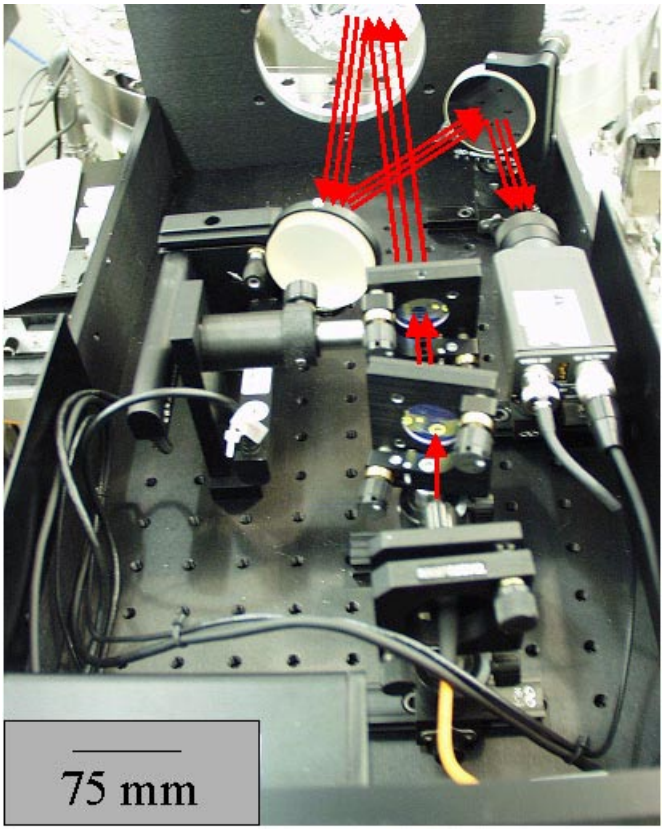

Figure 9. Two views of the MOSS system used for erbium hydride experiments. It includes a laser, two etalons, a rapidly switched, tiltable mirror assembly and a CCD camera.

Substrate preparation and erbium hydride thin film deposition procedures

Films are reactively sputtered onto a number of different substrates in order to determine the influence of starting surface structure. Substrates include α Al_2O_3 {0001}, α Al_2O_3 {11$\underline{2}$0}, Si(100) having native oxide and polycrystalline Mo. All samples are initially diced into 12mm x 37 mm or 12mm x 50 mm rectangles and wet-chemically cleaned before loading. Cleaning of aluminum oxide (sapphire) involves sequential rinsing in acetone, deionized H_2O, hot hydrogen peroxide and deionized H_2O. Samples are blown dry with filtered nitrogen after rinsing.

Samples are loaded into the growth apparatus, and the system is evacuated for 12 hours prior to bakeout. The chamber including the gas manifold is then baked to 150^{o}C over 9 hours and allowed to cool. Films are deposited the following day after an extensive sample outgassing/equilibration procedure. Outgassing consists of a programmed 'ramp and hold' sequence including anneals at 50, 150, 300 (2 hours) and 500^{o}C (15 minutes). Substrates are controlled at the growth temperature for 1.5 hours before commencing growth. Prior to each deposition the Er target is presputtered for 15 minutes with H_2 flowing. This removes oxide that formed during air exposure and equilibrates deposition rate for sputter deposition in the presence of hydrogen. A shutter is placed between the sample and the Er target during each presputter.

The sputter gun parameters include a 1200eV beam energy (exiting source) and a 45mA beam current. Growth rates are approximately 0.35 Å/sec. A stable ion gauge measures the chamber pressure during sputtering, equal to 8.0 x 10^{-4} Torr. Immediately following deposition, the boralectric heater supply and the mass flow controllers are turned off. The chamber pressure rapidly decreases following deposition, attaining 1.0 x 10^{-6} Torr in 1 minute.

Purity of erbium hydride thin films

Several analysis techniques show that 1200 Å – thick sputtered metal hydride thin films are relatively free of impurities. Rutherford backscattering spectrometry (RBS) and elastic recoil detection (ERD) demonstrate that films consist mostly of Er and H. RBS spectra, such as the ones shown in Figures 10 and 11, indicate the presence of Er in the film and Al and O confined within the substrate. Most importantly, RBS spectra indicate no large amount of oxygen in the bulk of films. The presence of oxygen within films would be indicated by higher backscatter yield at energies greater than that corresponding to the displayed oxygen front edge (channel 200). As indicated in Figure 11, RBS spectra reveal small amounts of Ar in the bulk of films. Ar is incorporated during deposition, when using Ar as the sputter gas. Similar amounts of Ar are retained in films grown at 30-400^{o}C.

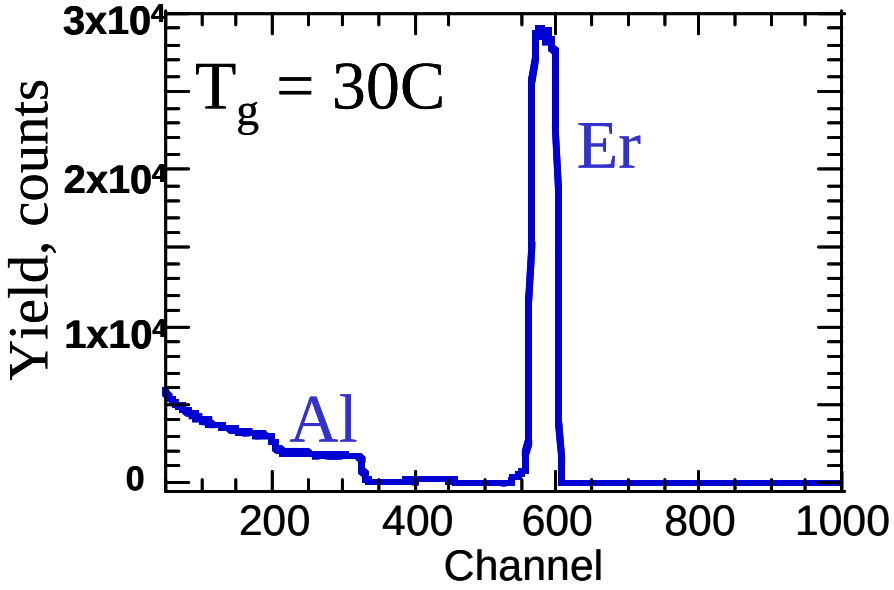

Figure 10. Rutherford backscattering spectra taken from an ErH_3 film grown at 30°C.

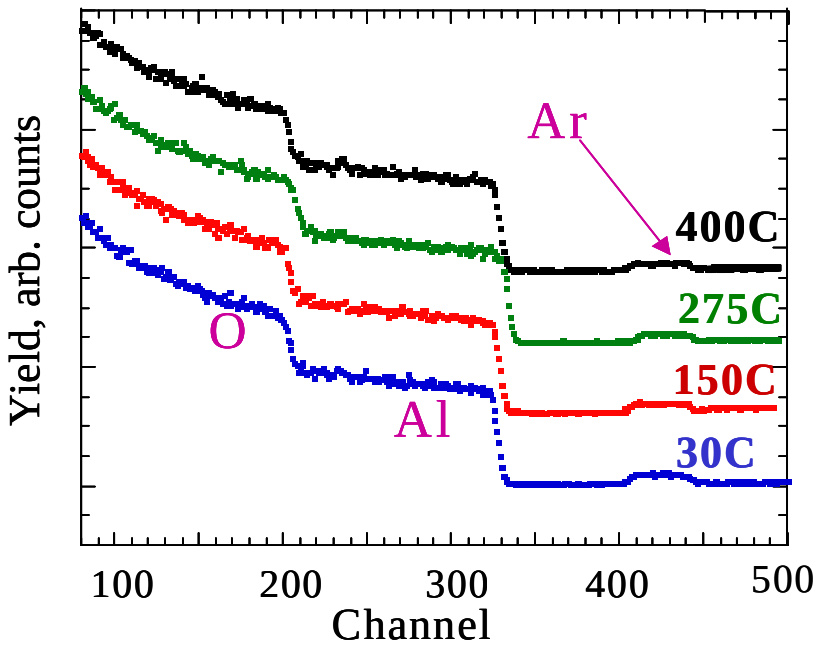

Figure 11. Low mass constituents as indicated by RBS. The temperatures listed are the growth temperatures.

Auger electron spectroscopy (AES) depth profiles confirm that films are compositionally pure. AES indicates that the bulk of films consist of Er with relatively little oxygen, as summarized in Table 1. Films grown at 400°C or less contain less than 1% oxygen. Slightly larger amounts of oxygen are found in films grown at 430°C, 460°C and 500°C. Oxygen in these films likely originates from intermixing with sapphire substrates at higher growth temperatures or outgassing of the heater assembly. The impurity levels listed in Table 1 are typical of films grown on sapphire. Growth on Si at 275°C or lower temperatures similarly results in a pure film with negligible amounts of oxygen, although significant Si – Er intermixing occurs at 500°C. The oxygen concentrations are estimated from the measured Er/O peak height ratios taken from differentiated Auger spectra. For these measurements we use the ratio of Er[MNN]/O[KLL] with sensitivities for Er = 0.067 and O = 0.247. Sensitivities are determined from numerous measurements of an erbium oxide standard. Note, the reported oxygen concentrations listed in Table 1 account for the presence of hydrogen. Although AES cannot detect H, we factor in its concentration measured by elastic recoil detection. Films are analyzed using a Physical Electronics PHI 660 scanning Auger system. A 5keV electron beam is employed with ~ 400nA beam current. Sputtering for depth profile analysis involves 3keV Ar.

Growth Temperature, °C	Estimated oxygen concentration (at.%)
30	<1.0
150	<1.0
270	<1.0
400	≤1.0
430	5.0
460	9.0
500	13.0

Table 1. Purity of erbium hydride films deposited by reactive sputtering onto Al_2O_3 {11$\underline{2}$0} substrates. Deposition is conducted in the presence of hydrogen with the ECR source removed.

Typical AES depth profile concentration maps are shown in Figure 12 for films grown at two different temperatures, 275 and 400°C. The films described in these plots are deposited onto {11$\underline{2}$0} sapphire and have thicknesses of approximately 1200 Å. While each film develops a thin surface oxide, no significant amount of oxygen accumulates in the bulk. Films are also inspected for the presence of other potential contaminants, such as N, Fe, C, Ar, Cr, and Ni, but no evidence of these species is detected.

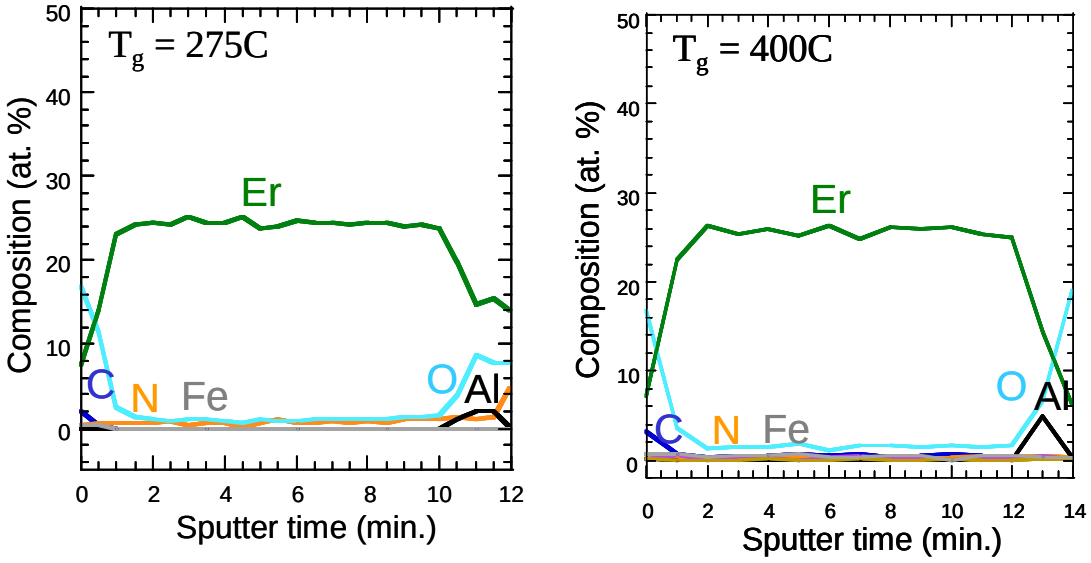

Figure 12. AES depth profiles through entire film thickness. Plots show that an oxide forms at the surface of a film; however, only trace amounts of oxygen are detected in the bulk.

Hydrogen /metal ratio of sputtered thin films

The hydrogen / metal ratio of all films is probed using ERD and RBS. RBS measures the areal density of Er using a 2.0 MeV beam of ^{4}He, an incidence angle of 10^o from sample normal, and a backscatter (detector) angle of 164^o. A typical RBS spectra is shown in Figure 10. ERD analysis determines the areal density of H. ERD measurements involve a 24 MeV Si^{5+} beam, a 75^o incidence angle (relative to sample normal) and a 12 μm thick Mylar range foil. Representative ERD spectra are shown in Figure 13 for three growth temperatures. Measurements of Er and H areal density are conducted using the same EN tandem van de graaff accelerator and analysis chamber. This helps to minimize error in determining relative amounts of these two species.

Rutherford backscattering spectrometry and elastic recoil detection analyses determine the H/Er ratio in films for different growth temperatures. As indicated in Figure 14, the ratio of measured areal densities, η_H / η_{Er}, is 3:1 for films grown at 30, 150, 275^{o}C. Above 275^{o}C the ratio of H/Er decreases, and at a growth temperatures of 460^{o}C, η_H / η_{Er} is approximately 2:1. Note, erbium hydride films are initially probed 1-3 weeks after growth, but several are analyzed six months after deposition. No change in the H/Er ratio is detected after long time. Error bars indicated in the plot for the H/Er ratio reflect the uncertainty of measurements by ion beam analysis. Accurate measurements of H areal density by ERD are made possible with a silicon nitride

standard that contains 5.77 x 10^{21} H/cm^3, or ~6.0 at.%.For completeness, we list the measured H/metal ratios in Table 2.

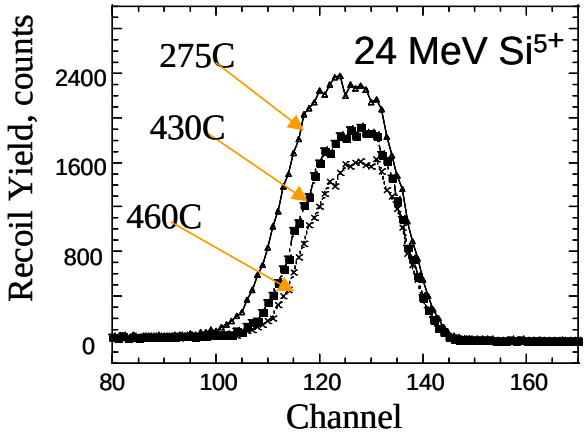

Figure 13. Elastic recoil yield for ErH_x films grown at various temperatures.

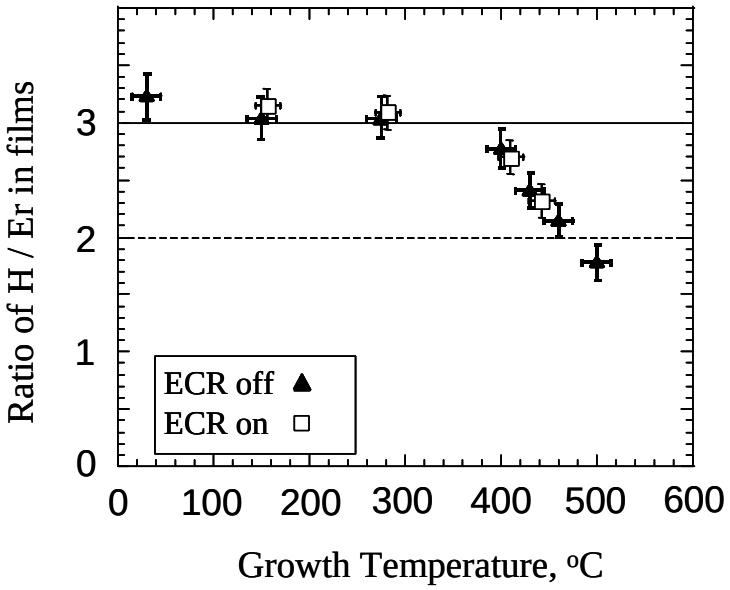

Figure 14. Ratio of H/Er in reactively sputtered erbium hydride films versus growth temperature. Measurements are taken from films grown onto sapphire substrates. The results shown include films grown with the ECR on and off.

Deposition Temperature, ^{o}C	Ratio of H/Er in deposited films
30	3.2 $\pm$ 0.2
150	3.0 $\pm$ 0.2
270	3.0 $\pm$ 0.2
400	2.8 $\pm$ 0.2
430	2.4 $\pm$ 0.2
460	2.15 $\pm$ 0.2
500	1.8 $\pm$ 0.2

Table 2. Summary of H/metal ratio in reactively sputtered erbium hydride thin films (not using ECR source).

Crystal phase, texture and microstructure of sputtered erbium hydride thin films

In order to identify the phase of reactively sputtered erbium hydride thin films, we first use x-ray diffraction (XRD) to probe crystal lattice spacings. A custom built micro-diffractometer system having a Siemens Hi-Star area detector is used to collect x-ray diffraction data. With this instrument, we scan from 20-50^{o} 2θ, while probing a range of χ between –20 to +20^{o} about the surface normal. This system employs a Rigaku 12kW rotating anode (Cu) as the x-ray source, and the x-ray beam is collimated using a 100 μm diameter pinhole. A nickel foil attached to the front surface of the area detector filters K_{β} radiation.

Area detector patterns such as the one shown in Figure 15 (on left) are acquired for each thin film. Integrating a small slice through the area detector maps, generates the 1-D diffraction scans shown in Figure 15 (on right). Although scans cover a large range of 2θ, only a portion of the data is plotted about the sole diffraction peak detected. As shown in the figure, a single Bragg reflection is found at 2θ=29.7^{o} for films grown at 30, 150, and 275^{o}C. The diffraction peak centroid is located at slightly larger 2θ for growth at 400 and 430^{o}C. The single diffraction peak in each scan is consistent with a {111} reflection for the cubic hydride structure having a d-spacing of 3.00 Å at low T_g and 2.97 Å at higher T_g. The predicted ErH_2 {111} lattice spacing is 2.96 Å based on a unit cell dimension of 5.12 Å. It is apparent that films are not hexagonal considering the significantly large range of 2θ between the predicted positions of the hexagonal reflections and the observed peak position. The 2θ values for the hexagonal phase and the {111} reflection of a strain-free fluorite lattice are shown at the top of the first plot in Figure 15.

These data are interesting, for x-ray diffraction indicates that films have a cubic metal sublattice despite a large H/Er ratio. This is surprising considering that the H/Er ratio is 3:1 for several growth temperatures below 400^{o}C, and at equilibrium (and moderate pressure) a hexagonal lattice is expected for this stoichiometry.

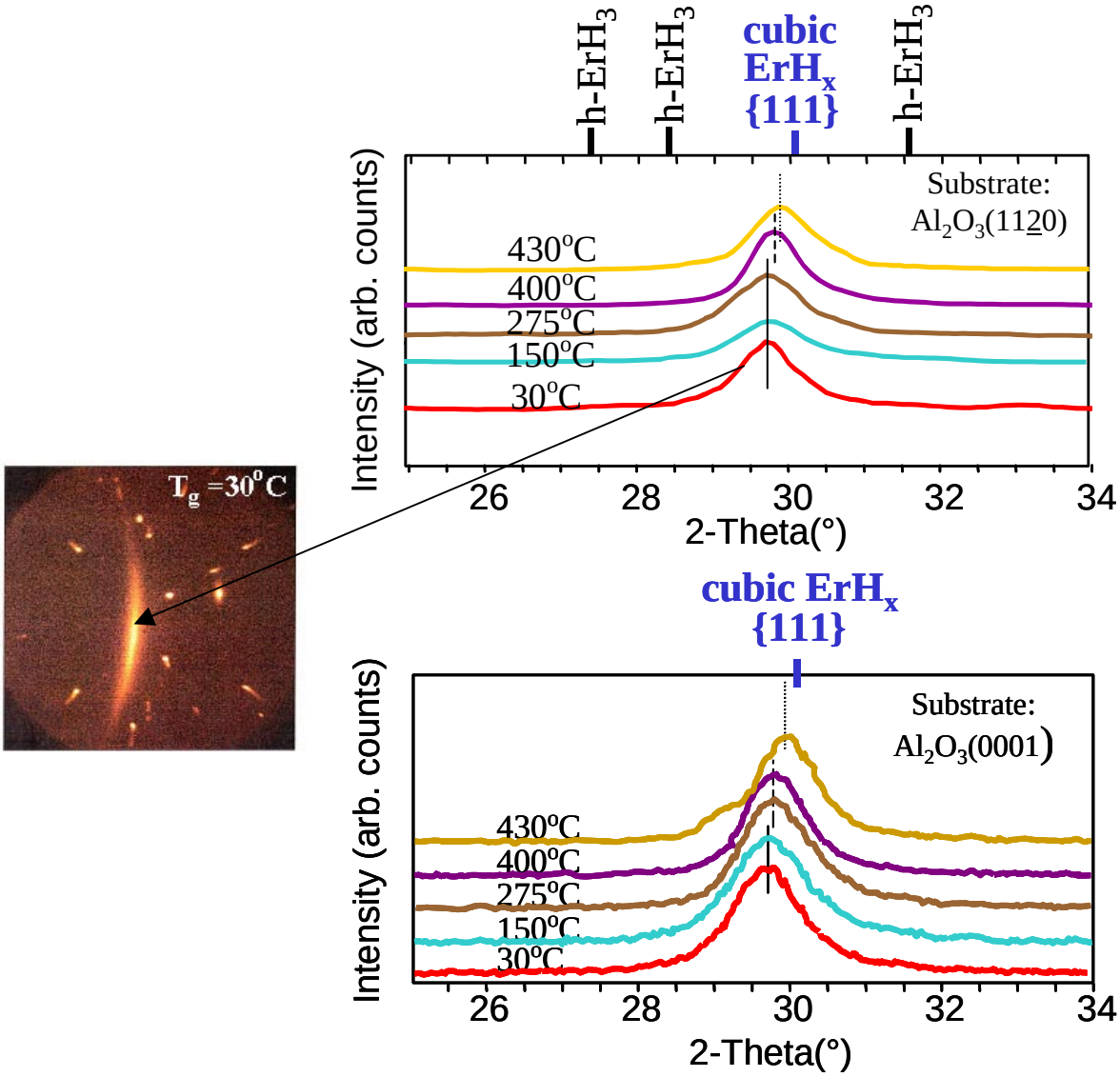

Figure 15. XRD scans taken from a set of erbium hydride thin films sputter deposited onto two sapphire surfaces. A single peak is observed over a range of 2 theta (20-50°) consistent with an out-of-plane texture. Known 2-theta values for the hexagonal ErH_3 phase (denoted 'h-ErH_3') are shown relative to the known {111} reflection of the cubic (fluorite) lattice.

A cubic metal sublattice structure is consistently found independent of the substrate material or its crystallographic orientation. Figure 15 shows the XRD scans taken from two sapphire substrate surfaces – the {0001} and {11$\underline{2}$0} planes. Almost identical information is obtained from these two sets of data. These are consistent with XRD data taken from ErH_x films grown onto Si(100) and Mo substrates for T_g = 30 and 150°C.

The XRD scans also show that films have a consistent out-of-plane crystallographic texture. The presence of a single peak over a range of 20-50 degrees demonstrates that films are textured in the <111>. This too is consistent for all substrate materials and orientations tested.

X-ray pole figure techniques probe over a larger range of reciprocal space in order to determine crystal type and to study out-of-plane and in-plane film texture for different substrate materials. In these experiments 2θ is varied incrementally by 0.25^{o} between 25-36^{o}, and a complete pole figure to $\chi = 80^{o}$ is scanned *for each* θ. Representative pole figures are shown in Figure 16 for films grown onto three different substrates. All detected Bragg reflections originating from the metal hydride films are consistent with a single-phase, cubic structure. In addition to a detected {111} reflection, diffracted radiation is observed in pole figure experiments at $2\theta \sim 35.0^{o}$ – consistent with the {200} lattice planes of a cubic phase. Interestingly, no evidence of a hexagonal ErH_3 crystal structure is found in any ion beam sputter deposited film. Potential ErH_3 reflections that fall within the range of angles probed are calculated to be at $2\theta = 27.3^{o}$, 28.4^{o} and 31.6^{o} for CuK_{α} radiation ($\lambda = 1.54$ Å).

From these pole figures it is also apparent that films form a strong {111} out of plane texture for different substrate materials. The {111} planes are tilted slightly with respect to the wafer normal direction, as indicated by the position of the <111> central pole. Pole figures of films grown onto sapphire and Si at higher temperatures are included in Appendix 1.

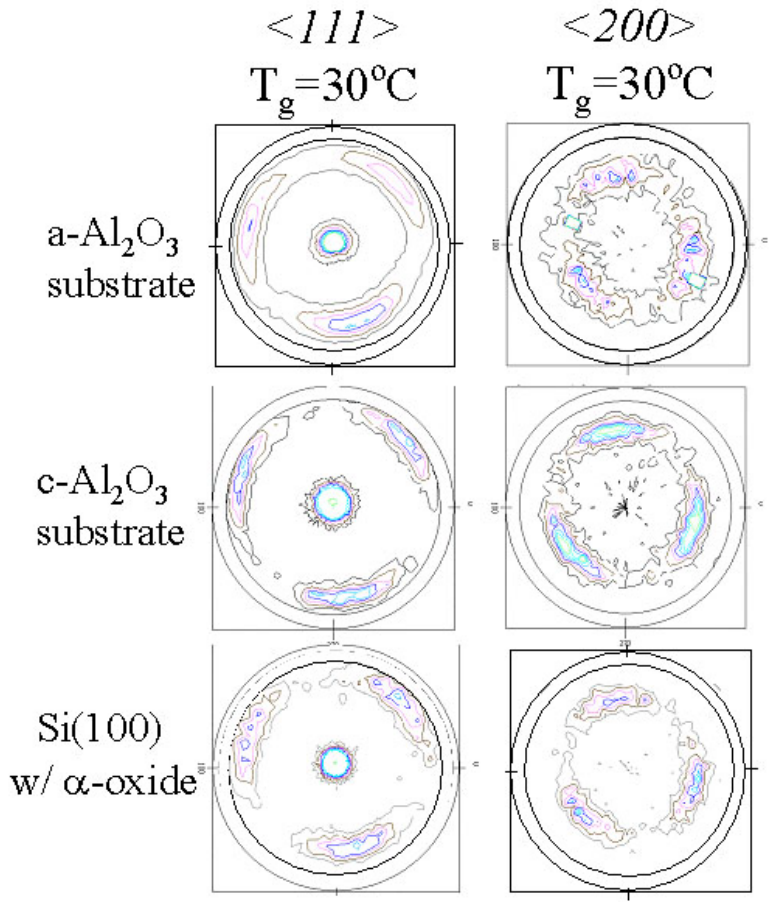

Figure 16. <111> and <200> pole figures taken from films grown onto various substrate surfaces. Substrates include crystalline $Al_2O_3\{11\underline{2}0\}$ (denoted 'a-Al_2O_3') and $Al_2O_3\{0001\}$ (denoted 'c-Al_2O_3') and an amorphous substrate surface (denoted 'Si(100) w/ α–oxide').

In addition to a strong <111> out of plane texture, pole figures taken from numerous erbium hydride films demonstrate a moderate in-plane texure (see Figure 17). An in-plane texture is indicated by the presence of lobes (discontinuous rings) in both the <111> and <200> pole figures. This texture forms for all films grown onto sapphire at 30, 150, 275, 400, 430 and 460^{o}C. The same in-plane texture is found for erbium hydride deposited onto Si at 30, 150 and 275^{o}C (see Appendix 1, 2nd page).

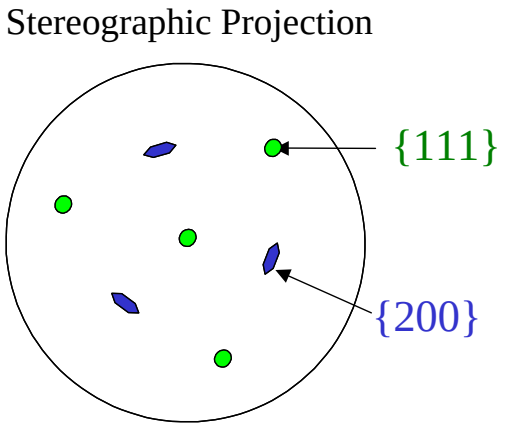

Figure 17. Stereographic projection summarizing relative orientation of diffraction maxima for <111> textured films.

Although initially we suspected epitaxy was responsible for the in-plane texture of films grown onto Al_2O_3{0001} (since this surface had a common symmetry with the indicated pole figure), analysis of films deposited onto Si(100) having an *amorphous* oxide confirm that other factors are important. Note, deposition of erbium hydride at 30 and 150^{o}C does not compromise the native oxide of Si. This is demonstrated by a high-resolution, cross-section TEM image shown in Figure 18.

We explain the common in-plane thin film texture by a break in the deposition symmetry. In-plane texture develops in sputtered thin films due to the sample /target geometry. In our experiments substrates and the sputter target are fixed; however, their relative orientation is such that the metal flux has an oblique incidence angle. An explanation of in-plane texture based on obliquely incident deposition flux is consistent with the work by Karpenko et.al.[23] In that research, sputtered film texture was studied for various static and dynamic deposition geometries. In general, their work demonstrates that deposition geometries (including those with rotation) having a net oblique component of the flux lead to in-plane texture in metal films. This included growth onto amorphous surfaces.

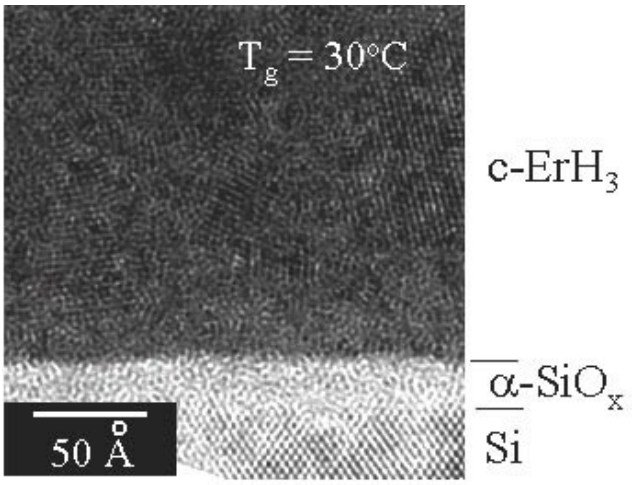

Figure 18. A high resolution cross-section TEM image of a cubic ErH_3 film (denoted c-ErH_3) deposited onto the native oxide of silicon. At a growth temperature of 30°C the amorphous oxide (labeled as α-SiO_x) remains intact.

Transmission electron microscopy (and electron diffraction) is also used to evaluate crystal phase. Consistent with the XRD and pole figure experiments, we again find evidence for a new phase: cubic erbium trihydride. For this, a second set of films that showed a hydrogen/metal ratio of 3 are thinned and inspected in a transmission electron microscope using diffraction. As shown in Figure 19, a number of diffraction rings originating from the cross sectioned film are used for comparison against known lattice reflections of the hydride phases. The measured lattice spacings of 1.48, 1.54, 1.82, 2.58 and 2.97 Å compare favorably with the known lattice spacings for the cubic phase shown on the right. The measured lattice spacings do not match those of a hexagonal trihydride phase, Er or Er_2O_3. The known lattice spacings of hexagonal ErH_3 and Er_2O_3 are listed in Appendix 2. Consistent with x-ray diffraction and pole figures, TED shows a {111} out of plane texture in sputtered films. Superposed on the electron diffraction pattern in Figure 19 are spots originating from the alumina substrate. This particular diffraction pattern is taken along the {0001} zone axis.

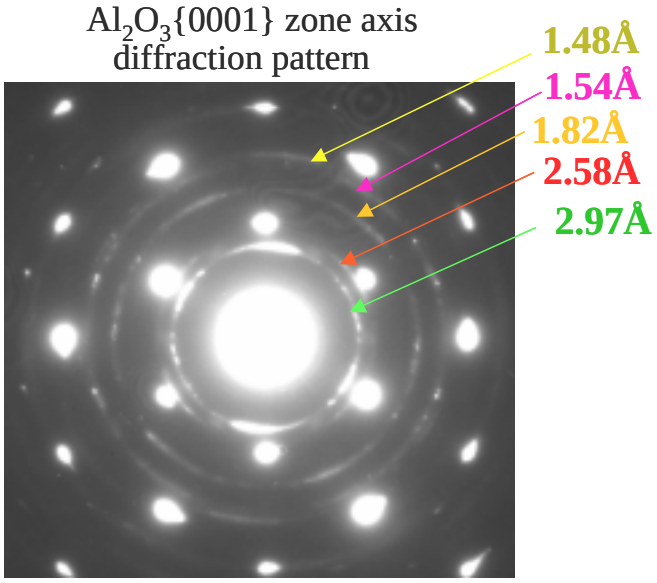

a.

Reflection	Lattice spacing
(111)	2.96 Å
(002)	2.57 Å
(220)	1.81 Å
(311)	1.54 Å
(222)	1.47 Å

b.

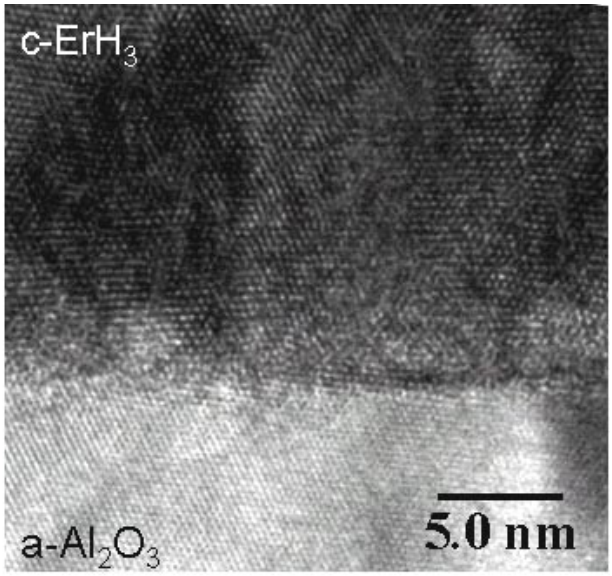

c.

Figure 19: a. Transmission electron diffraction pattern taken from an erbium hydride film deposited onto Al_2O_3{11$\underline{2}$0} at 30°C. Also listed in a. are measured lattice spacings. b. lists the allowed reflections for electron diffraction and known lattice spacings for the cubic erbium hydride phase (typically having a composition of ErH_2). c. shows a high resolution TEM image of the film / substrate from which the pattern was obtained. 'c-ErH_3' denotes cubic erbium trihydride.

Transmission electron microscopy is used to probe the grain structure of 1200 Å thick erbium hydride films. In general, films develop a columnar microstructure as shown in Figure 20 for growth on sapphire. Films consist of extremely fine grains independent of substrate material. We estimate the average grain size at 2-15 nm. This is consistent with the large width of diffraction peaks detected by XRD for all growth temperatures. A plan view TEM image of a film grown on sapphire is also shown in Figure 21 . Appendix 3 shows similar grain structure for growth on Si(100).

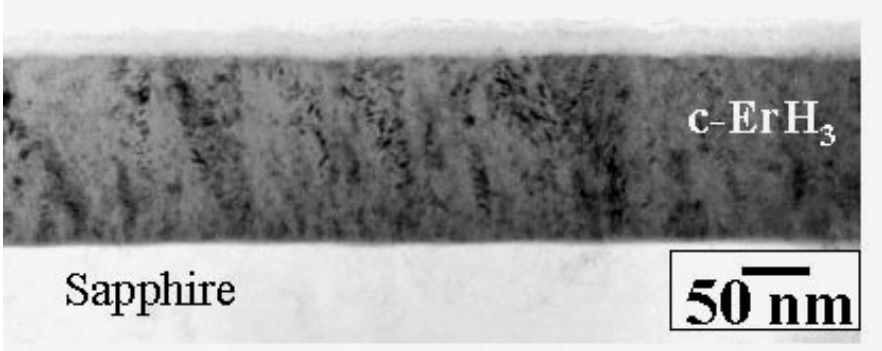

Figure 20. Cross-section TEM image (bright field) of an ErH_3 film deposited onto sapphire at 30°C.

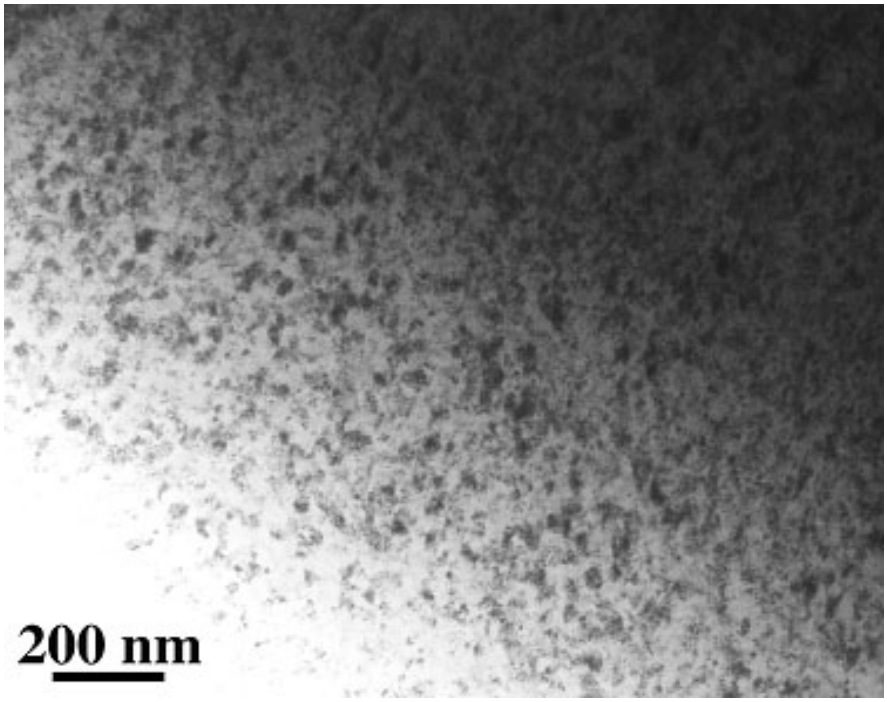

Figure 21. Plan view TEM image of an ErH_3 film deposited onto sapphire at 30°C.

In summary, x-ray diffraction, pole figure analysis and transmission electron microscopy demonstrate the same crystal phase and similar microstructure for films grown at 30, 150, 275 and 400°C onto sapphire substrates. Films grown at these temperatures have a cubic metal sublattice structure, and there is no apparent intermixing with sapphire substrates. This latter point is confirmed by cross section TEM.

On the other hand, for growth temperatures of $\geq$ 430°C, different phases and microstructures develop. XRD of 1200 Å thick erbium hydride films does show evidence of a cubic hydride phase for growth temperatures as high as 500°C (see Figure 22). In addition, films grown at 430, 460, 500 and 525°C develop a second phase - Er_2O_3. This is consistent with the elevated oxygen levels shown in Table 1 for high growth temperatures.

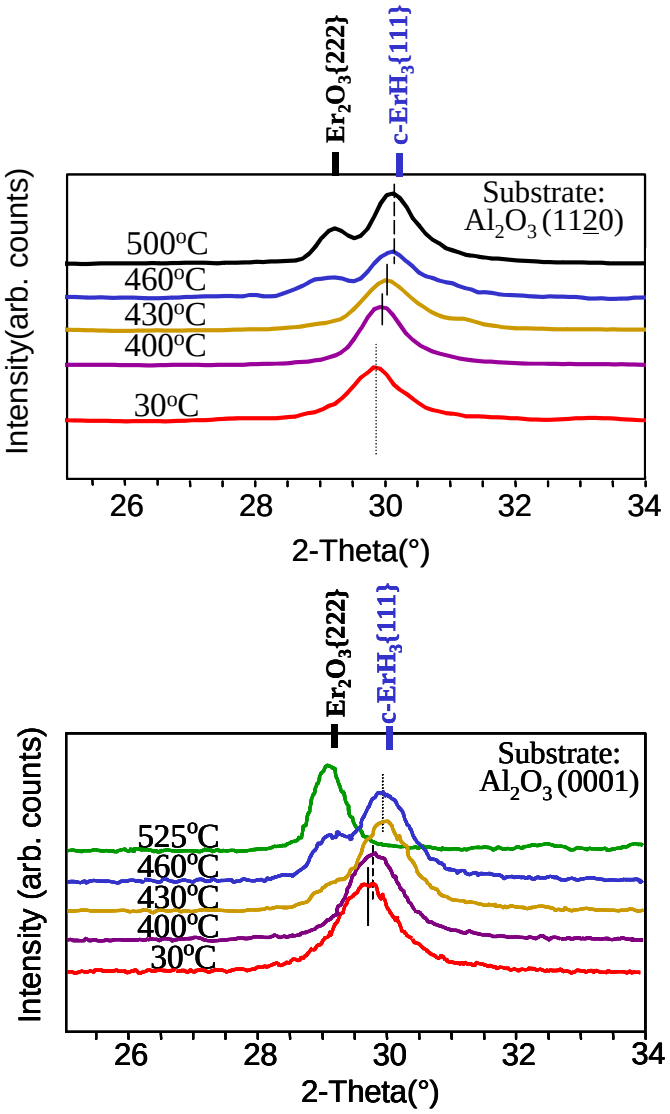

Figure 22. XRD scans of films grown at several high temperatures and at 30°C (for comparison). Evidence of Er_2O_3 is found for growth temperatures above ~430°C. 'c-ErH_3' denotes cubic erbium trihydride.

In order to investigate the extent of intermixing and the structure formed near the film – substrate interface, we cross-section a number of films deposited onto sapphire. Cross-section TEM shows that films deposited at 430^{o}C or higher interact to a large degree with the substrate to form aluminum oxide. Figure 23 shows three cross section TEM images of films grown at 400, 430 and 460^{o}C. For increasing growth temperature we find a larger mixed volume near the film – substrate interface. TEM and composition analysis show three distinct features in films grown at 430^{o}C and higher temperatures. These are labeled in Figure 23 as A, B and C. Feature C consists of cubic erbium hydride and some erbium oxide. Feature B consists mostly of aluminum and has a low density. Feature A has sizeable microvoids; the bright features in region A show Fresnel contrast.

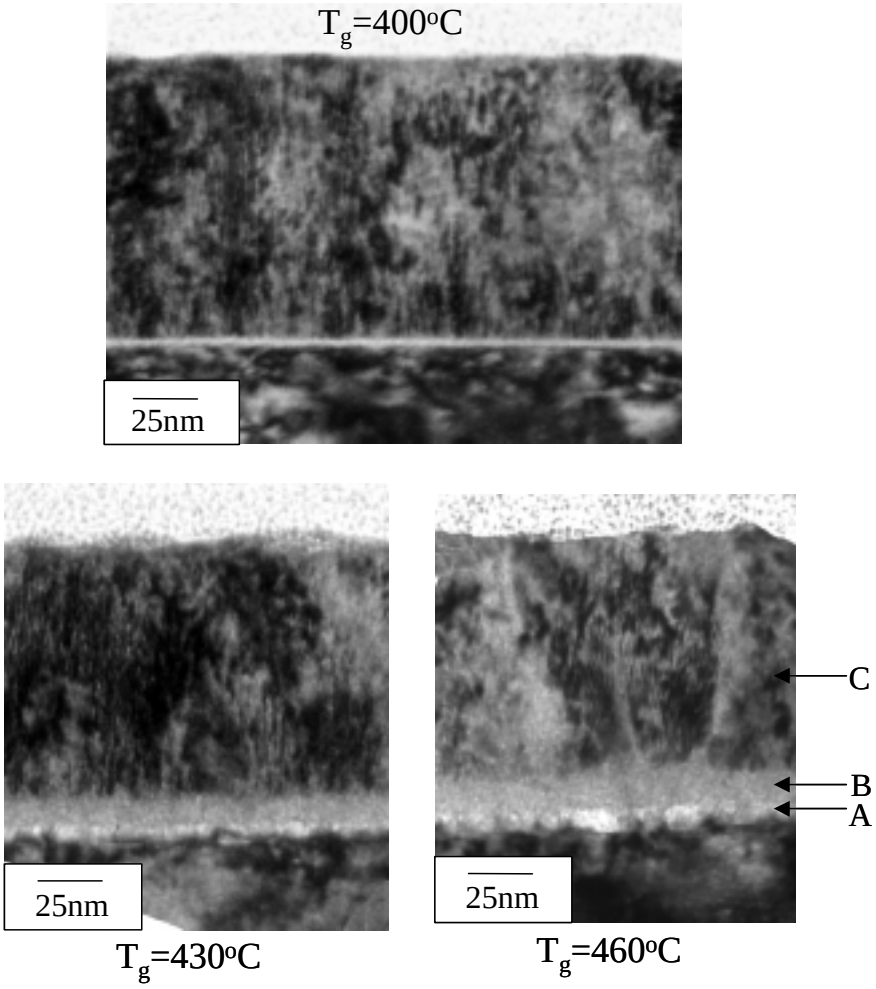

Figure 23. Cross section TEM images of sputtered erbium hydride films deposited at several higher temperatures. Evidence of Er_2O_3 is found for growth at temperatures of 430^{o}C or higher.

Our experiments suggest that erbium oxide forms at higher growth temperatures because of intermixing with the aluminum oxide substrate. Oxygen is found in the bulk of films grown at higher temperatures, with the concentration of oxygen increasing with higher growth temperature. Based on the TEM evidence which shows an increasingly thick intermixed layer near the original film – substrate interface with higher T_g, we do not expect that substrate/holder outgassing contributes significantly to the formation of erbium oxide in films. To test this assumption, we conducted a deposition onto a polycrystalline molybdenum surface and analyze its purity. Sputter deposition of erbium hydride onto molybdenum results in a cleaner deposit.

Reduction of the alumina substrate to form erbium oxide is not surprising considering the enthalpies of formation for aluminum oxide (ΔH_f^o = -1675 kJ/mol) and erbium oxide (ΔH_f^o= -1898 kJ/mol).[24] We predict that features A and B result from considerable reduction of the alumina substrate.

Sputtered erbium hydride thin film stress

In order to better understand sputtered metal hydride films and the origin of a cubic erbium trihydride phase, we analyze the evolution of film stress. An *in-situ* technique (MOSS) is used to investigate the evolution of stress, including intrinsic and extrinsic effects.

A standard laser alignment/ baseline acquisition procedure is used prior to all depositions. First, the laser is stabilized for 0.5-1.0 hour prior to data collection. With the sample at the growth temperature, we then obtain a baseline measure of wafer curvature by opening the shutter to the sample (sputter gun off). A baseline scan is acquired for 10-15 minutes, and, provided that no changes in curvature occur over this time, we proceed to deposit. Two directions are always probed on a wafer as indicated in Figure 24. As discussed earlier, rectangular substrates are clamped at one end in a springboard configuration with deposition flux covering the entire sample length except for a small area near the clamp. The spot pattern is aligned on the sample prior to deposition by viewing through a second port. A 2x3 array of spots is used for all experiments, and care is taken to position the spot array at least 2mm from each sample edge.

Baseline scans taken prior to each deposition allow determination of the sensitivity for curvature measurements. The minimum resolvable curvature is calculated from the mean differential spot spacing $\langle \Delta D/D_o \rangle$ observed for fixed temperature with no deposition flux impinging on a substrate. For this analysis, we take a mean differential spot spacing to be twice the standard deviation of the signal fluctuations. We spatially average over all measured spacings to calculate one mean spacing and hence one minimum resolvable curvature. In general, we find approximately the same high sensitivity, regardless of substrate temperature. κ_{min} is approximately 0.0001 m^{-1} for a $\langle \Delta D/D_o \rangle_{static}$ equal to 0.0002. This is similar in both horizontal and vertical directions. All measurements are made with the vacuum system cryopump operating. The formulation relating mean differential spot spacing to curvature is [25]

$$\Delta D(t)/D_o = (2L/\cos\alpha)\kappa\,(t)$$

where L is the sample – camera path length and α is the incidence angle of the laser light. From changes in curvature, the stress can be determined using Stoney's equation

$$\sigma_f t_f = M_s t_s^2 \Delta\kappa / 6$$

where σ_f is the stress in the film, t_f is the film thickness, M_s is the biaxial modulus of the substrate, t_s is the substrate thickness, and $\Delta\kappa$ is the change in curvature.

We find that for our current sample holder assembly, substrates are in a near biaxial condition in the area monitored for curvature. To test this, we deposit an erbium hydride thin film and monitor the curvature in the horizontal and vertical directions as shown below. A Si(100) substrate is chosen, because the {100} plane of silicon is elastically isotropic. This means that the measurements made in two orthogonal directions should be identical if the sample is in a biaxial state. As shown in Figure 24 a small difference (~10%) is, however, detected in two orthogonal directions. We plot the 'apparent film stress' in this figure, or that calculated based on the changes in curvature in the two directions. The stress calculated in the horizontal direction is reduced compared with that determined along the vertical direction of the substrate. Since we have no reason to believe that there is a difference in how a film grows in the two orthogonal directions (aside from an in-plane texture), we expect that the observed difference in curvature is a result of a near-biaxial condition imposed by the sample holder/clamping arrangement. A similar effect is found by others[26] when using a rectangular substrate /springboard configuration.

Because there is a detectable difference in our setup, all analyzed data sets for our research are reported in terms of the more accurate direction.

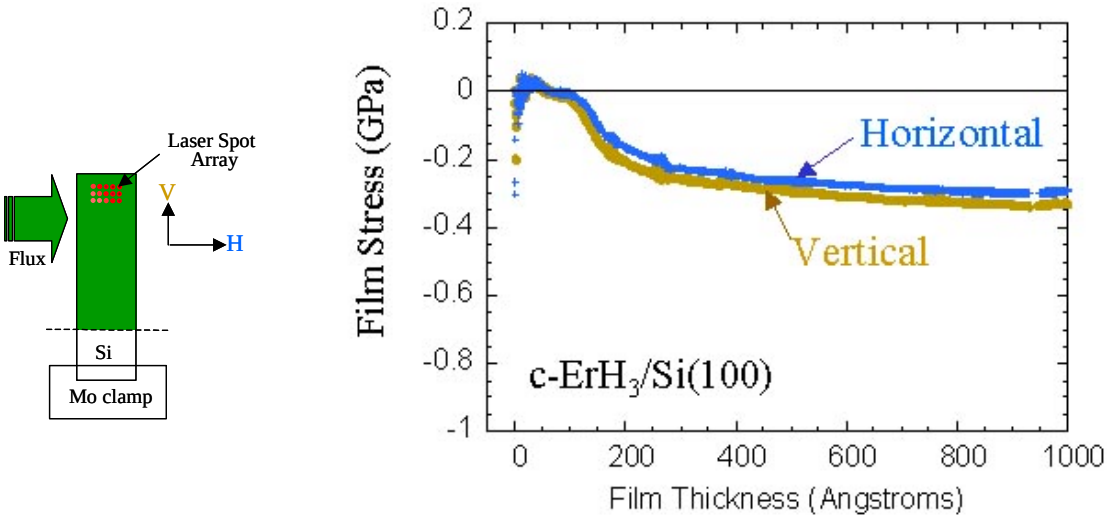

Figure 24. Plot of apparent film stress acquired during deposition onto Si(100) substrate having a native oxide. Graph shows the apparent stress calculated from measurements of wafer curvature changes in two orthogonal directions as shown. The small difference between the two curves indicates a near-biaxial condition. The shorter of the two sample sizes (12mm x 37 mm) is chosen for the control experiment.

Figure 25 shows the evolution of stress during ion beam sputter deposition of erbium hydride thin films onto sapphire and cooldown. This includes measurements for three growth temperatures, 30, 150 and 400°C. To recall, films grown at these three temperatures show evidence for a single phase – cubic erbium hydride with a nominal composition of ErH_3. Additionally, these films develop an identical out-of-plane and in-plane texture. Plots of stress during fabrication have similar features including: a compressive–tensile–compressive transition at the early stages of deposition, a large compressive stress during the remainder of film growth, and a reduction in compressive stress immediately following growth as the sample is cooled.

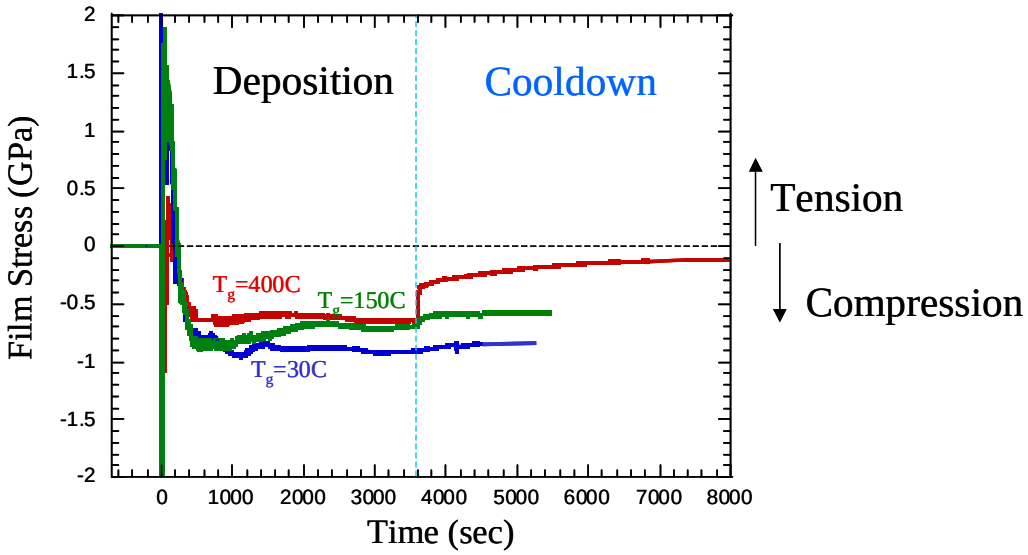

Figure 25. Evolution of stress during ion beam sputter deposition of erbium hydride thin films and cooldown. Results are shown for three growth temperatures. Al_2O_3 {11$\underline{2}$0} substrates are used. A modulus of 551 GPa is used for calculating stress from curvature; the procedure for determining modulus is listed in Appendix 4.

Although the stress developed in the early stages of deposition (thicknesses ~ few monolayers) is not considered important for metal hydride applications that target thick films, the data shown in the first part of Figure 25 displays some features that are of general interest. These are also presented in a second plot – Figure 26. During the first 75 Å of film growth there are several changes in stress state. All films grown onto sapphire show a large compressive stress during the first 25 Å depending on growth temperature. The peak compressive stress is difficult to quantify, but is on the order of 1-2 GPa. After attaining a large compressive stress, films exhibit a transition to a tensile state. In some cases the magnitude of the tensile stress is large (~ 1 GPa). The stress of films then evolves to a compressive state at approximately 75 Å. It attains a near-constant compressive stress after ~ 250 Å of film growth.

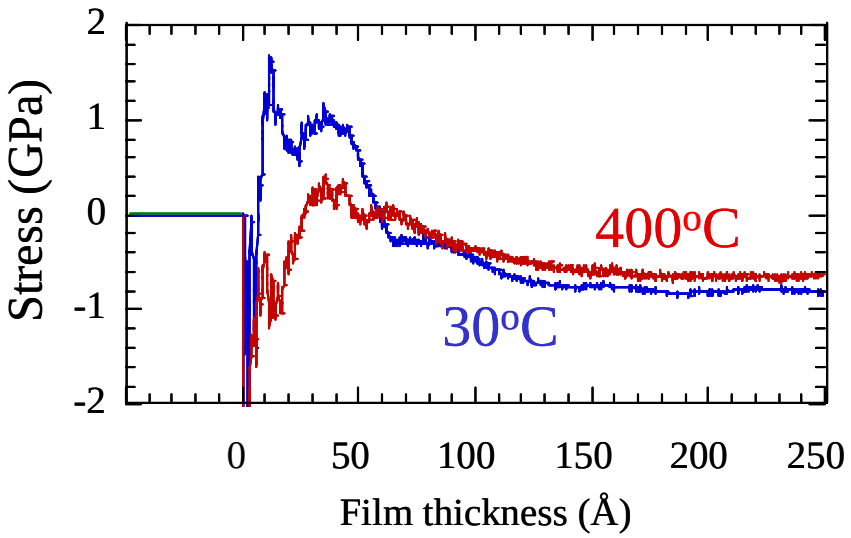

Figure 26. Evolution of stress during ion beam sputtering of erbium hydride thin films. Results are shown for two growth temperatures and highlight the changes in stress that occur during the earliest stages of growth.

We expect that the compressive-tensile-compressive (CTC) behavior is similar in origin to that found for other Volmer-Weber growth mode[27] thin film systems.[28,29] In general, CTC transitions in stress[30] correlate with island nucleation and growth, island coalescence, and postcoalescence growth.[31] At the earliest stage of growth, films consist of discrete islands. Islands present a surface stress that originates from the local bonding environment experienced by atoms composing a thin film of partial coverage.[32] As additional flux arrives, islands begin to coalesce. When islands impinge upon other islands, free surfaces are transformed into grain boundaries. A reduction in surface energy accompanies this conversion, leading to a tensile stress. It has been shown that a peak in the tensile curvature occurs when the film becomes fully continuous.

We point out that the large stress changes that occur during the early stages of erbium hydride sputter growth are very different than those fluctuations shown at large thicknesses for ScD_2 deposition (involving two-step processes). It is emphasized that the changes in stress during this earliest stage of sputter deposition do not affect the mechanical integrity of a thick metal hydride film. It is true that films attain large stresses on the order of a GPa. However, the large changes in stress displayed in Figures 25 and 26 occur in the earliest stages of growth, corresponding to monolayer-type coverages. The stress developed is a consequence of the transition from 'nucleation to growth' on a surface. In many respects, it is the 'inverse process' of cracking, as islands are zipped together during coalescence.

In-situ analysis indicates erbium hydride films are in a state of compression throughout deposition following the first few monolayers of growth. As shown in Figure 25, the stress of films is between 0.6 and 0.85 GPa after the first 400 sec of growth (~ 120 Å). Similar trends are observed for deposition onto Al_2O_3 {0001} as well as Si (see Appendix 5).

A compressive stress in thick films is not surprising considering that ion beam sputter deposition is used for growth. Ion beam sputter deposition typically results in compressively stressed films.[33] Explanations of this prevelant stress state commonly link compression to a low pressure in the sputter chamber during growth and high momentum species (reflected Ar neutrals and sputtered Er atoms) incident on a growing film.[34] Early explanations of compressively stressed, thick deposits built on the idea of energetic particle bombardment to explain the origin of compression as 'atomic peening'.[35] More recent work on compressively stressed sputtered films considers the various microstructural features that compose a film. For example, research by Ramaswamy et. al.[36] and a recent model by Chason et. al.[37] identifies grain boundaries as an important factor in generating a compressively-stressed, continuous film.

After deposition is complete, the flux (H_2, Ar and Er) and substrate heater are turned off simultaneously. It is during cooldown from T_g that ion beam sputter deposited films show a reduction in compressive stress. The magnitude by which the stress is reduced depends on the growth temperature. Films grown at low T_g (30^{o}C) maintain a large compressive stress whereas films grown at 400^{o}C have dramatically lower stress. For all growth temperatures studied, films remain in a state of compression once ambient temperature is attained. Note, the differences in residual stress as a function of growth temperature indicated in Figure 25 (by MOSS) are in agreement with the post-growth XRD data shown in Figure 15. XRD θ-2θ measures out-of-plane strain.

We expect that extrinsic effects, i.e., a difference in CTE for substrate and film, lead to a compressive stress reduction during cooldown. Sapphire substrates have a coefficient of thermal expansion ($\alpha = 7.7 \times 10^{-6}/^oC$)[38] that is approximately 0.5x that of erbium hydride.[39] Based on this difference in α, one would predict a less compressive, or possibly tensile, film stress upon cooling. Furthermore, films grown at high temperatures show the largest decrease in compressive stress; almost no change in stress is found after deposition at 30^{o}C. This is also consistent with a prediction of stress change based solely on CTE mismatch.

Nevertheless, we are aware of recent research by Floro et. al.[30] and others[40] that identifies additional factors which may contribute to a stress change immediately following growth. As demonstrated for other materials systems, curvature changes are observed during growth interrupts at fixed temperature. These changes in stress are explained by a change in the chemical potential at the film surface as the flux is turned off.[37] Because our procedure at the end of deposition is to simultaneously turn off the heater supply and flux, we cannot separate out the effects of extrinsic stress and this recently identified mechanism using the data in Figure 25. Nevertheless, we find minimal changes in curvature after films are deposited at 30^{o}C. We consider this important, for it suggests that changes in stress during cooldown is affected mostly by

extrinsic effects. Additional growth interrupt experiments are required to determine whether the effects of a changing chemical potential are more important at higher growth temperatures.

In order to determine whether a difference in CTE plays a dominant role in affecting stress immediately following growth at high temperature, we use the data acquired by MOSS to estimate a coefficient of thermal expansion for erbium hydride and compare this to known values measured previously by XRD.[39] We use the 'cooldown' portion of the $T_g = 400^oC$ data set to extract a measure of the CTE. We assume that the stress change with temperature is governed by the following equation:

$$\frac{d\sigma}{dT} = M_f * (\alpha_s - \alpha_f)$$

where

$\frac{d\sigma}{dT}$ is the derivative of stress versus temperature

M_f is the biaxial modulus of the film (for isotropically elastic material = $E/1-\nu$)

α_s is the substrate thermal expansion coefficient

α_f is the film thermal expansion coefficient

An additional approximation and assumption are made for this analysis including

1. the CTE, α_s, for aluminum oxide is constant over the range of temperatures probed and equal to $7.7 \times 10^{-6}/^oC$, and

2. Poisson's ratio, ν, of the film is equal to 0.3.

Previous nanoindentation experiments by N. Moody (SNL) show that the indentation modulus, $E/(1-\nu^2)$, of erbium hydride is equal to 282 GPa. Using $\nu = 0.3$, the biaxial modulus of the film, $E/(1-\nu)$, is calculated to be 367 GPa.

Figure 27 shows the evolution of stress during erbium hydride thin film fabrication for $T_g = 400^oC$. In addition, the plot on the lower half of the figure shows only changes in stress during cooldown from T_g. These changes are plotted versus temperature. A reasonable fit to the data provides a measure of the CTE for erbium hydride (in this case $ErH_{2.8}$) equal to $12.1 \times 10^{-6}/^oC$. The previously measured value for ErH_2 averaged over a range of temperatures is $16.0 \times 10^{-6}/^oC$. It is our opinion that the value measured by MOSS is in reasonable agreement with that

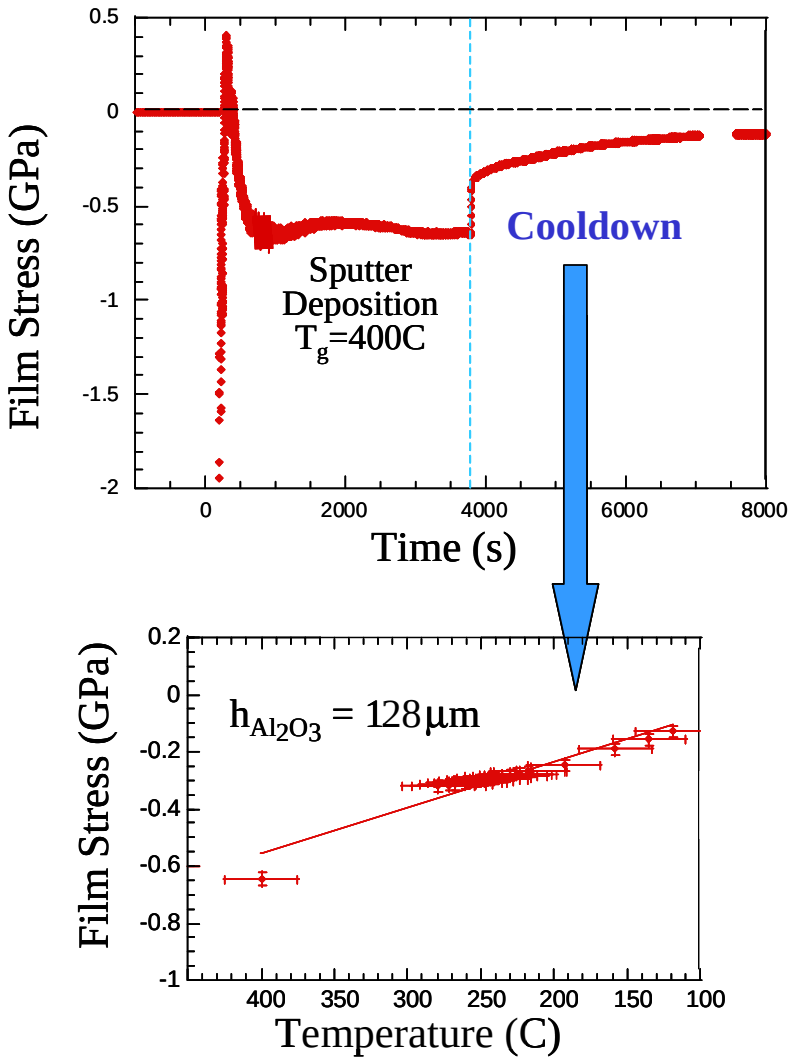

Figure 27. Plot (top) displays the evolution of film stress during fabrication of erbium hydride involving reactive sputter deposition. Plot (bottom) shows only those changes in stress that occur during cooldown from the growth temperature, 400°C.

determined previously. This implies that extrinsic effects are largely responsible for the changes in stress that occur immediately following deposition at high temperature.

Discussion of strain energy stabilization

Several sets of data presented in this report indicate that ion beam sputter deposited films form a newly-discovered cubic erbium trihydride structure. In this section we briefly discuss whether a compressive film stress should contribute to the development of this crystallographic phase. A high compressive stress (i.e., internal pressure) could lead to an increased film density. Given the right circumstances, such as a fine-grained thin film microstructure which can tolerate extremely high stress, compression could also induce a phase change. A high-pressure phase would also have a higher density by comparison to other candidate structures. Note, there are several examples of strain energy stabilized thin film and bulk phases, including a high-pressure phase of scandium hydride – ScH_3.

As a first step toward predicting the stability of a cubic erbium trihydride phase, we calculate and compare the densities of the candidate phases. As listed in Table 3, the phases considered include hexagonal ErH_3 and cubic ErH_3. The lattice parameters shown for the first phase are taken from previous measurements on strain-free trihydride crystals.[12,13] The atomic density for cubic ErH_3 is calculated in two ways. The first estimates the density based on a cubic lattice parameter of 5.10 Å. This is used, because cubic films grown at T_g = 400°C are measured to have this lattice spacing. The second calculation for cubic ErH_3 uses the lattice parameter measured by diffraction for films grown at T_g = 30-275°C. Transmission electron diffraction shows the in-plane lattice spacing of these sputtered thin film crystals to be a = 5.08 Å.

Stoichiometry	Metal sublattice structure	Lattice parameter(s)	Density (at./ Å^3)
ErH_3	Hexagonally close packed	a = 3.63 Å ; c = 6.54 Å	8 atoms/74.62 Å^3 *= 0.107 atoms/ Å^3*
ErH_3	Face centered cubic	a = 5.10 Å	16 atoms/132.7 Å^3 *= 0.120 atoms/ Å^3*
ErH_3	Face centered cubic	a = 5.08 Å	16 atoms/131.1 Å^3 *= 0.122 atoms/ Å^3*

Table 3. Estimated atomic densities for hexagonal ErH_3 and cubic ErH_3. Also shown are the lattice parameters used for the calculation.

Table 3 shows that a cubic erbium trihydride phase has a larger atomic density compared with the hexagonal trihydride phase. The density is greater irrespective of the two lattice parameters used for the calculations. This supports the observation of a strain energy stabilized cubic trihydride thin film.

Section V: ***Reactive deposition of scandium deuteride***

Reactive deposition is also researched as a method for depositing stoichiometric scandium hydride (ScD_2) thin films. In this set of experiments, we deposit scandium metal by evaporation. Relevant to this work we anticipate that this technique will provide better control of near-zero residual stress compared with two-step metal hydride fabrication processes highlighted in Figures 1 and 2. Evaporated films and those grown by reactive methods, often have low stress. Similar to work on erbium hydride, a challenge of this research is to control stress while maintaining required stoichiometries (hydrogen/metal ratio) and high purity. Ultra-high vacuum techniques are paramount; scandium has a strong affinity for oxygen.

Scandium hydride deposition and analysis system

The system used for reactive deposition of scandium deuteride thin films is an ultra-high vacuum cryopumped apparatus referred to as 'Evap 1' (see Figure 28). The chamber is a water-cooled stainless steel, vertical cylinder with a volume of 60 liters. While the system is designed for all metal seals, a Viton o-ring is used on the lid seal for all experiments. All additional seals remain metal. The system is roughed entirely with dry vacuum pumps to < 50 mTorr before crossing over to a CTI Cryogenics CT8 cryopump. Typical base pressure attained after an overnight bakeout is $<10^{-8}$ Torr. For reactive deposition, scandium is evolved from a single-pocket electron beam evaporator in the presence of molecular deuterium. A crystal monitor rate controller regulates the electron gun power for a constant deposition rate. For all experiments a thin Cr layer is deposited prior to the significantly thicker scandium deuteride coating. Films are grown to a ~'1x' thickness.

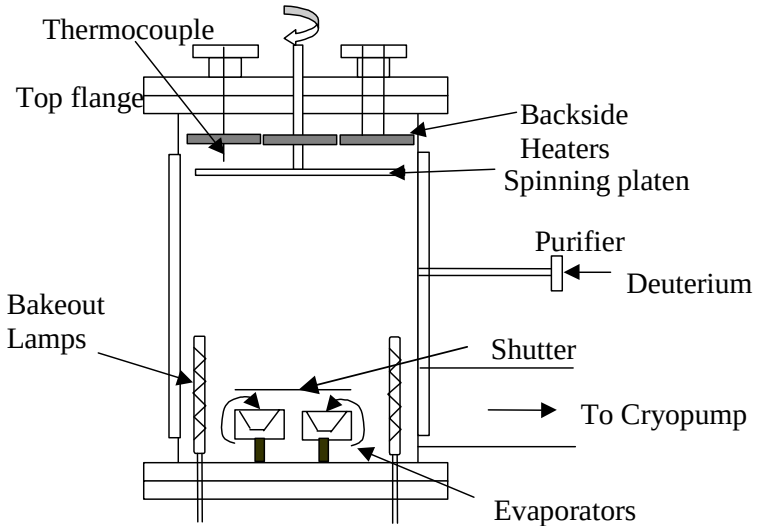

Figure 28. Schematic of reactive deposition apparatus used for depositing ScD_2.

Substrates rest on a stainless steel platen that is rotated by a UHV bellows type feedthrough located in the center of the top plate. Samples are rotated to improve the deposition uniformity and provide uniform heating. This platen can hold up to 20 3.75 cm diameter substrates and is made planar with the top plate flange for ease of MOSS laser alignment. The chamber has two heater arrangements. Substrate heating is provided by three 10 cm Boron Nitride-encased graphite heaters located behind the wafers at a spacing of 3 cm. These heaters are controlled by closed loop temperature feedback from a type K thermocouple located 6mm from the backside of the platen. Two infrared bakeout lamps located in the bottom of the chamber accomplish chamber bakeout. Prior to each process run the chamber is baked out over several hours at a substrate temperature of 200ºC and a wall temperature near 100ºC.

Deuterium is introduced into the chamber in order to grow stoichiometric ScD_2. Gas is delivered to the middle of the chamber through a 3/8" stainless steel tube after passing through a palladium membrane purifier. The purity of the initial gas is 99.9995% research grade deuterium. Vendor specifications indicate impurity levels of < 1 ppm H_2O, < 1 ppm O_2, and < 1 ppb hydrocarbons/halocarbons as delivered from the purifier. Additional in-line filters are incorporated into the deuterium gas feed line to ensure high purity deuterium is introduced into the system during deposition. Since the deuterium-loaded metal will outgas upon subsequent heating (e.g., during bakeout), all shields and fixtures are replaced after each run. These parts are stripped of chromium and scandium with a dilute ceric ammonium nitrate solution and rinsed. All parts are then solvent cleaned, followed by a bake in hydrogen and in vacuum to 800ºC prior to returning for use in the evaporator system.

A second MOSS system is incorporated onto Evap 1 for experiments that monitor scandium deuteride thin film stress. The apparatus is different than the instrument used for ErH_x experiments, for it probes the curvature during sample rotation (for deposition) and with samples stationary (for cooldown). This instrument also uses a two-dimensional array of laser beams to noninvasively monitor stress. Film stress is monitored in these particular experiments by scattering laser light off the backside of substrates, i.e., side opposite of the deposition flux. Therefore, semi-transparent substrates such as sapphire are coated on the backside with a reflective metal layer. Previous work[9] shows that this method of 'backside metallization' does not introduce artifacts in the stress curve falsely attributed to the stress of scandium dideuteride. Polished Mo-alumina cermet is sufficiently reflective and dose not require a coating on the back side.

Additional features are incorporated onto the chamber and MOSS unit for improved stress analysis. This includes a rotary encoder and software that correctly triggers a CCD camera to probe the same region on a moving substrate. A 12-bit programmable shaft encoder is connected to a vacuum feedthrough that attaches to the spinning sample platen. This encoder has 4096 counts per 360^o (an angular resolution of 0.087^o / count). The encoder count that corresponds to a centered substrate is determined and recorded prior to each experiment and referenced throughout. Note, this count is different in static versus dynamic mode. A communication signal delay time is taken into

account when samples are rotating to ensure that the same wafer area is monitored throughout an experiment.

Modified software allows for monitoring of multiple substrates (up to eight) during a single deposition. In addition, a rapidly switched, tiltable mirror that accounts for small differences in sample alignment on a platen is added. This aids in experiments that probe multiple samples in one deposition event and is useful for locating reflected laser spots prior to an experiment without removing the MOSS cover. A schematic of our revamped MOSS system is shown in Figure 29.

The sensitivity in measuring curvature (and stress) for different operations is also determined for this chamber/MOSS setup. The minimum resolvable curvature is calculated from the mean differential spot spacing $\langle \Delta D/D_o \rangle$ observed for fixed temperature with no deposition flux impinging on a substrate. The highest sensitivity is found while samples are kept stationary and at low temperature. κ_{min} is approximately 0.0001 m^{-1} for a $\langle \Delta D/D_o \rangle_{static}$ equal to 0.0002. Slightly decreased sensitivity is found at higher substrate temperatures. In dynamic mode, sample rotation leads to a lower sensitivity, approximately equal to 0.001 m^{-1}. Most likely platen eccentricity and wobble during spinning give rise to this higher noise level. All measurements are made with the cryopump operating.

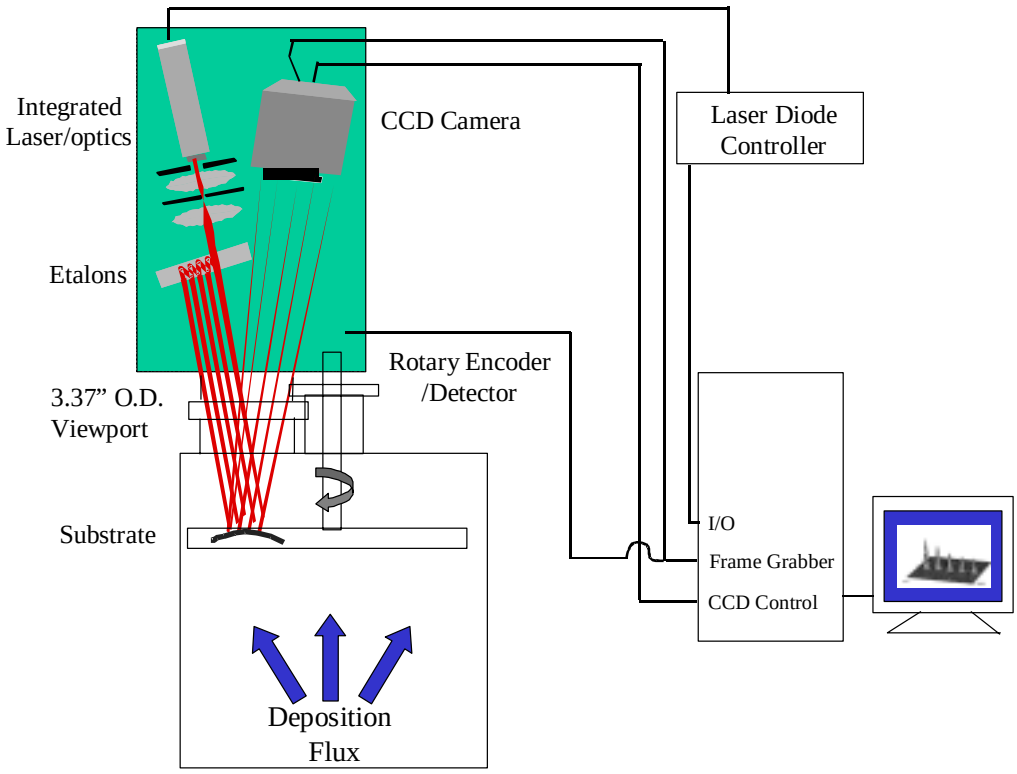

Figure 29. Schematic of a multi-beam optical stress sensor (MOSS) system designed to probe substrate curvature during sample rotation or while fixed.

Scandium deuteride thin film growth experiments

Several scandium deuteride thin films are grown by reactive techniques in order to determine whether evaporation in the presence of molecular hydrogen leads to better control of a near-zero stress film. Substrates for growth include cermet, sapphire and Mo witnesses. For each wafer material, it is essential to choose a substrate thickness that permits a detailed study of stress. Previous work determines wafer thicknesses appropriate for detecting a change in stress during two-step scandium hydride fabrication processes. We use the same batch of wafers (and wafer thicknesses) for the current experiments. The details of cermet and sapphire wafers are listed in Table 4. Cermet wafers are fabricated at Sandia National Laboratories from cermet CND50 powder. CND50 cermet contains 50 wt% (27 vol%) Mo.

Material, Diameter	Wafer Supplier	Wafer Thickness, h_s,	Roughness, R_a, on Film Growth Side	Biaxial Modulus, M (GPa)
Sapphire, R-plane (1$\underline{1}$02), 37 mm	Bicron-Saint/Gobain Crystal, Inc.	325μm (0.013")	300-350 nm	562*
Mo-alumina cermetCND50, 25 mm	Sandia National Laboratories	400μm (0.016")	40 nm	421 333 (nanoindentation)

** R-plane sapphire is not elastically isotropic in the plane of the film. The modulus specified for this substrate represents the value calculated from the Al_2O_3 stiffness tensor for the R-plane in a direction perpendicular to the wafer flat.*

Table 4: Description of wafers used for reactive deposition of scandium deuteride.

Sapphire substrates are initially cleaned using a solvent rinse and baked in the growth system at 200°C for several hours and at 525°C for 5 minutes. Cermet substrates are solvent cleaned and, in a similar method, vacuum baked at 200°C and 525°C in the deposition system.

After samples are cleaned at high temperature the heaters are turned off and the samples are allowed to cool down to approximately 30°C. At this time, each substrate is measured to determine initial curvature represented by a zero mean differential spot spacing. A zero value of initial curvature does not imply that a wafer is perfectly flat initially (radius of curvature infinitely large). However, it is a reference for changes in curvature that develop during processing.

Sample growth temperatures are chosen to be 100-200°C, in order to avoid a large tensile stress upon cooldown after growth. Metal deposition rates are constant, and a fixed deuterium pressure between of 4×10^{-5} and 1.0×10^{-4} Torr is selected. Films

consist of a thin Cr underlayer and a much thicker (approximately '1x') scandium deuteride layer.

MOSS shows that a reactively deposited scandium dideuteride thin film of '1x' thickness can have minimal stress, compared with that formed by two-step fabrication processes. Figure 30 shows almost no change in sapphire wafer curvature during reactive scandium deuteride growth and cooldown. The plot shows a baseline curvature measurement, no detectable change in stress during reactive deposition and only a slight change in stress during cooldown. This is compared with the large changes in stress that develop during two-step processes involving metal deposition and hydriding – Figure 1. Note, the two figures are directly comparable; the same sapphire substrate thickness and crystallographic orientation is used for each experiment.

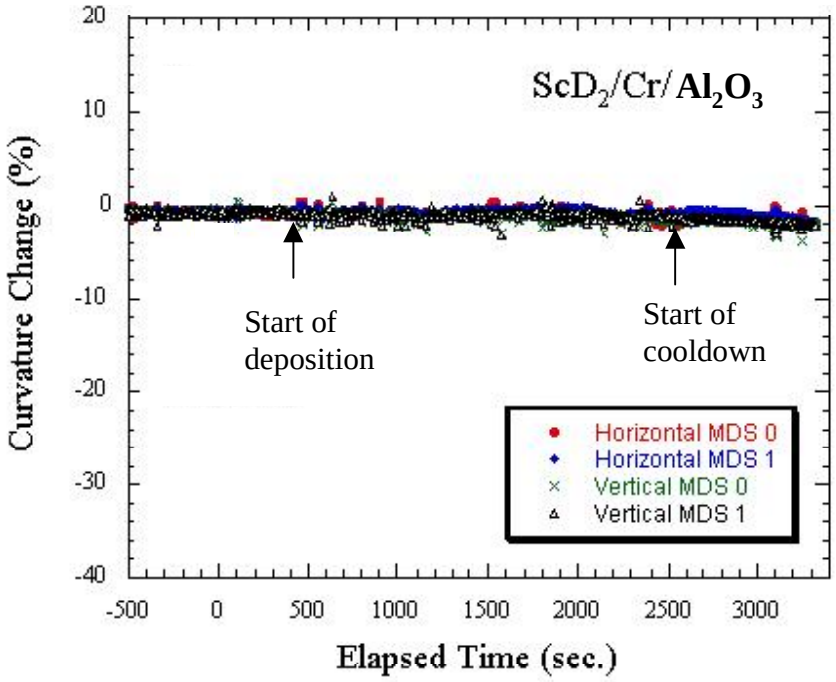

Figure 30. Evolution of film stress as determined by MOSS. Film is reactively deposited onto sapphire and has a measured composition of $ScD_{1.8}$. T_g= 115°C.

Films grown reactively onto cermet substrates also show minimal stress as detected by MOSS. This is demonstrated in Figure 31 for a '1x' film grown at 200°C having a composition of $ScD_{1.83}$. The near-zero stress shown in Figure 31 can be compared with that evolved during fabrication using a two–step process, shown in Figure 32. Note, the cermet substrates used for these separate experiments are taken from the same batch produced at SNL, and the substrate thicknesses are identical within 5%. (See Appendix 6 for a more detailed plot of the data shown in Figure 31).

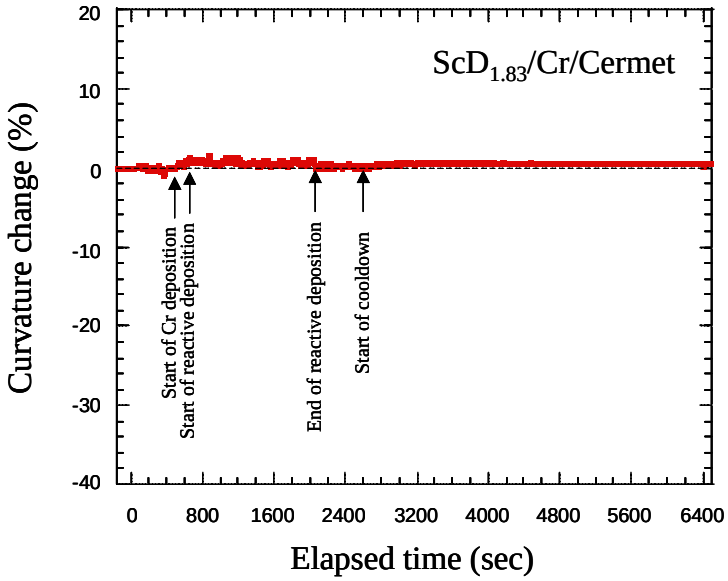

Figure 31. Plot showing minimal changes in cermet wafer curvature during reactive deposition of a '1x' scandium deuteride film. Film composition is $ScD_{1.83}$.

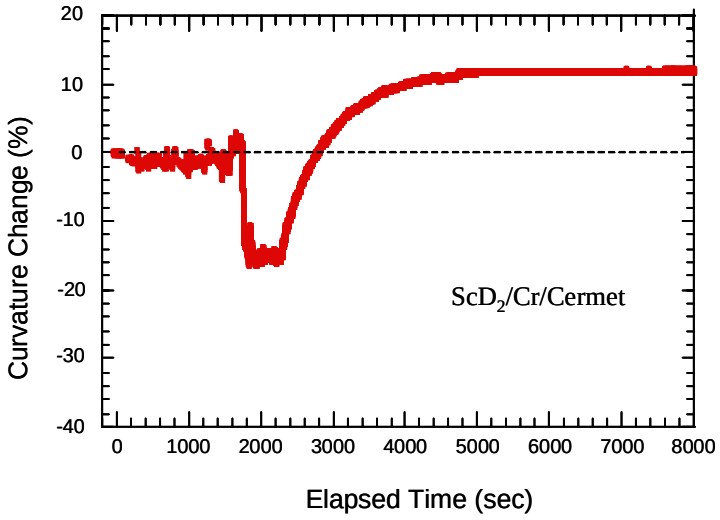

Figure 32. *taken from reference 9*. Plot of wafer curvature changes during deposition of a '1x' scandium deuteride thin film onto cermet using a two-step process of metal deposition and high temperature hydriding. This figure is included for comparison with the plot in Figure 31.

The composition and structure of reactively deposited scandium deuteride thin films is analyzed using ion beam analysis and XRD. In general, films are approximately '1x' in thickness. Additionally, films have large deuterium/ metal ratios in the range of 1.8-1.9. Stoichiometry (and thickness) is demonstrated in Figure 33 by comparing the D/metal ratio of a reactively sputtered scandium deuteride thin film to a standard of ScD_2. While the composition of films is just short of the desired dideuteride phase, the experiments are encouraging. Reactively deposited scandium deuteride films are confirmed by XRD to have the cubic dideuteride phase. This is to be expected considering the phase diagram for Sc – H shown in Figure 6. To recall, Manchester et. al.[15] explain that the (αSc+ δ / δ) boundary at room temperature is located at x=1.68 (62.7%H) for ScH_x. The boundary extends to lower values of x at higher temperatures, such as that used during deposition. We expect that improved UHV techniques, particularly more extensive bakeouts, source material outgassing and rigorous attempts to lower the base pressure would improve the stoichiometry, without affecting the near-zero stress. Each subsequent ScD_x reactive deposition experiment took more aggressive approaches toward cleaning the system prior to growth. As a result the hydrogen/metal 'load' ratio increased.

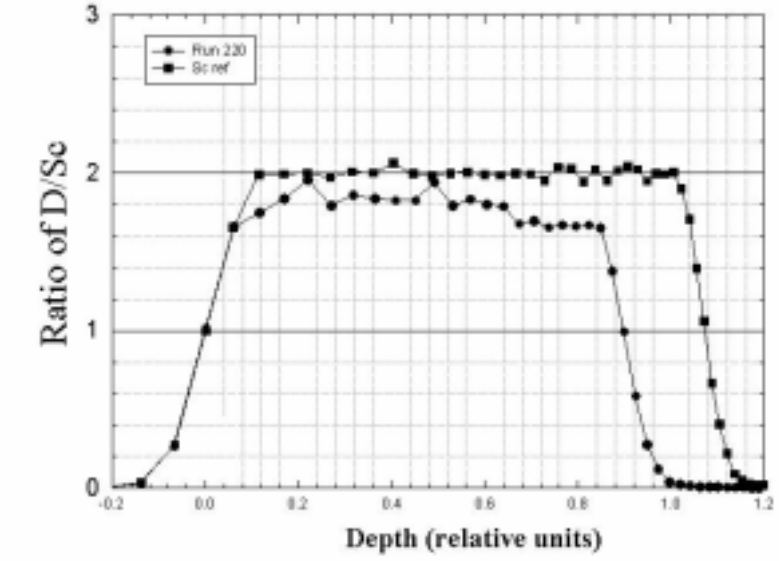

Figure 33. Representative plot of composition as a function of depth for reactively deposited scandium dideuteride film (●). This is compared with a reference standard sample (■). The average composition through the bulk of the film is $ScD_{1.8}$. Reactively deposited film analyzed is slightly less than '1x' thick.

CONCLUSIONS

In summary, erbium hydride thin films are reactively sputtered onto single crystal Al_2O_3, Si(100) with native oxide and molybdenum substrates at several temperatures. The microstructure, crystal phase, composition (hydrogen/metal ratio), purity and stress are evaluated. Interestingly, we find evidence for a new crystal phase: cubic erbium trihydride. Three diffraction techniques indicate that films grown at 30-400^{o}C have a cubic metal sublattice despite having a H/Er ratio of 3. X-ray pole figures, x-ray diffraction (using an area detector) and transmission electron diffraction show no evidence of the hexagonal trihydride phase. Rutherford backscattering and elastic recoil detection analyses reveal that the H/Er ratio is 3:1 at temperatures $\leq$ 400^{o}C and is closer to 2:1 at higher growth temperatures. All sputtered films grown below 400^{o}C are compositionally pure having less than 1 at. % oxygen. We have investigated the origin of the cubic hydride phase and currently explain it as a strain-energy stabilized crystal structure. Erbium hydride thin films grown by ion beam sputtering have a large in-plane compressive stress. This is determined by *ex-situ*, post-growth x-ray diffraction measurements of strain, and *in-situ* wafer curvature measurements of stress. All erbium hydride thin films are textured with a {111} out-of-plane crystal orientation. A moderate in-plane texture is found for growth on crystalline as well as amorphous substrates. This in-plane crystallographic alignment is due to the static deposition geometry employed and not epitaxy. It is suggested that future work explore further the stability of various metal hydride phases and the influence of strain energy and microstructure.

Scandium dideuteride thin films are also investigated, although to a lesser extent. Dideuteride thin films are grown by reactive deposition involving evaporation of scandium metal in the presence of molecular deuterium. Films grown to date have compositions in the range of $ScD_{1.8}$-$ScD_{1.9}$. For growth at 100-200^{o}C, MOSS indicates films have minimal stress compared with alternative two–step deposition techniques. Similar low stress films are expected upon achievement of desired ScD_2 – stoichiometry, when using reactive deposition techniques. Ultra-high vacuum methods are recommended for future work that aims to optimize the properties of reactively deposited erbium and scandium hydride thin films. Continued work will address alternative reactive sputter deposition techniques that provide even greater control of film stress.

REFERENCES

1. R. Griessen, J.N. Huiberts, M. Kremers, A.T.M. van Gogh, N.J. Koeman, J.P. Dekker, and P.H.L. Notten, Journal of Alloys and Compounds, **253**, 1997, 44-50.
2. J.N. Huiberts, R. Griessen, J.H. Rector, R.J. Wijngaarden, J.P. Dekker, D.G. de Groot, and N.J. Koeman, Nature, **380**, 1996, 231-234.
3. D.G. Nagengast, J.W.J. Kerssemakers, A.T.M. van Gogh, B. Dam, and R. Griessen, Appl. Phys. Lett., **75**, 1999, 1724-1726.
4. P. van der Sluis, M. Ouwerkerk, and P.A.Duine, App.Phys.Lett. **70**, 1997, 3356-3358.
5. G. Song, M. Geitz, A. Abromeit and H. Zabel, Phys.Rev.B, **54**, 1996, 14093-14101.
6. G. Andersson, B. Hjörvarsson, and P. Isberg, Phys.Rev.B, **55**, 1997, 1774-1781.
7. P.M.Reimer, H.Zabel, C.P.Flynn and J.A.Dura, Phys.Rev.B, **45**, 1992, 11426-11429.
8. Ch. Rehm, H. Fritzsche, H. Maletta and F. Klose, Phys. Rev. B, **59**, 1999, 3142-3152.
9. D.P. Adams, L. Brown, R. Goeke, J.A. Romero, B. Silva, *Evolution of Stress in ScD_2 /Cr Thin Films Fabricated by Evaporation and High Temperature Reaction*, SAND Report, (SAND2001-1629), 2001.
10. M.S. Rahman Khan, Thin Solid Films, **113**(#3), 1984, 207-213.
11. J.A. Grimshaw, F.J. Spooner, C.G. Wilson and A.D. McQuillan, J. Mat. Sci. **16**, 1981, 2855-2859.
12. W.M..Mueller, J.P. Blackledge and G.G. Libowitz, *Metal Hydrides*, (Academic Press, New York, 1968), pages 5, 432-434.
13. A. Pebler and W.E. Wallace, J. Phys. Chem. **66**, 1962, 148-151.
14. L.C. Beavis, J. Less Common Metals, **19**, 1969, 315-328.
15. F.D. Manchester and J.M. Pitre, J. of Phase Equilibria, **18** (2), 1997 194-204.
16. C.K. Saw, B.J. Beaudry, and C. Stassis, Phys. Rev. B, **27**, 1983, 7013-7017.
17. W.D. Nix, Metallurgical Transactions A, **20A**, 1989, 2230-2231.
18. D.P. Adams, L. Parfitt, J.C. Bilello, S.M. Yalisove, and Z.U. Rek, Thin Solid Films, **266**, 1995, 52. J. Tao, D. Adams, S.M. Yalisove, and J.C. Bilello, Mat. Res. Soc. Symp. Proc. **239**, 1992, 57.
19. E. Chason, J.A. Floro, J. Reno, J. Klem, *Final Report on LDRD Project: In Situ Determination of Composition and Strain During MBE*, SAND report, (SAND97-0295), 1997.
20. G. Stoney, Proc. R. Soc. London, Ser. A **82**, 1909, 172.
21. J.A. Floro, E. Chason, S.R. Lee, and G.A. Peterson, Appl. Phys. Lett. **71,** 1997, 1694.
22. S. Hearne, E. Chason, J. Han, J.A. Floro, J. Figiel, J. Hunter, H. Amano, I.S.T. Tsong, Appl. Phys. Lett. **74**, 1999, 356-358.
23. O.P. Karpenko, University of Michigan PhD Thesis, *Evolution of Surface Roughness and Texture During Low Temperature Film Deposition*, 1996.
24. *CRC Handbook of Chemistry and Physics*, Edition 79, (CRD Press, Boca Raton, 1998).
25. J.A. Floro and E.Chason, Mat. Res. Soc. Symp. Proc., **406**, 1996 491.
26. M. Finot, I.A. Blech, S. Suresh and H. Fujimoto, J. App. Phys, 81, 1997, 3457.
27. M. Volmer and A. Weber, Z. Phys. Chem. **119**, 1926, 277.

28. R. Abermann, R. Kramer and J. Mäser, Thin Solid Films, **5**, 1978, 215.
29. R. Abermann, Thin Solid Films, **186**, 1990, 233.
30. J.A. Floro, E. Chason, R.C. Cammarata and D.J. Srolovitz, **27**(1), MRS Bulletin 2002, 19-25.
31. J.A. Floro, S.J. Hearne, J.A. Hunter, P. Kotula, E. Chason, S.C. Seel, and C.V. Thompson, J. Appl. Phys. **89**, 2001, 4886.
32. R.C. Cammarata, T.M. Trimble, and D.J. Srolovitz, J. Mater. Res. **15**(11), 2000, 2468-2474.
33. H.Windischmann, J. Appl. Phys., **62**, 1987, 1800.
34. H.Windischmann, CRC Rev. in Solid State and Mat. Sci., **17**, 1992, 547-596.
35. F.M. D'Heurle, Metall. Trans. **1**, 1970, 725.
36. V. Ramaswamy. W.D. Nix (to be published) 2002.
37. E. Chason, B.W. Sheldon, L.B. Freund, J.A. Floro and S.J. Hearne, Phys. Rev. Lett. **88** ,2002, 6103.
38. T. Goto, O.L. Anderson, I. Ohno, and S. Yamamoto, J. Geophy. Res., **94**, 1989, 7588.
39. C.E. Lundin, R.C. Perkins and R.W. Sullivan, SAND Report, *X-ray Diffraction Study of Erbium-Hydrides, Deuterides and Tritides, submitted by University of Denver, Denver Research Institute* (SC-CR-67-2591X), 1967.
40. A.L. Shull and F. Spaepan, J. Appl. Phys. **80**, 1996, 6243.

APPENDIX 1:

<200> and <111> x-ray pole figures taken from erbium hydride thin films grown onto {11$\underline{2}$0} sapphire at various temperatures.

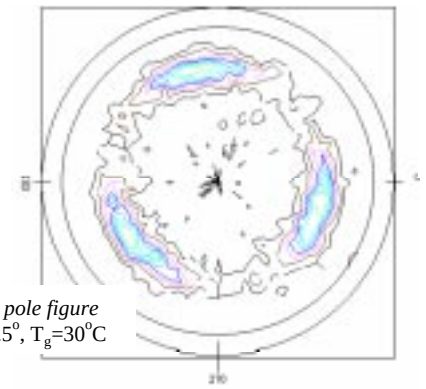

<200> pole figure
$2\theta = 34.5^{o}$, $T_g = 30^{o}C$

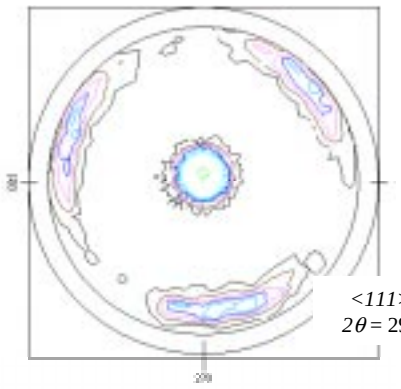

<111> pole figure
$2\theta = 29.7^{o}$, $T_g = 30^{o}C$

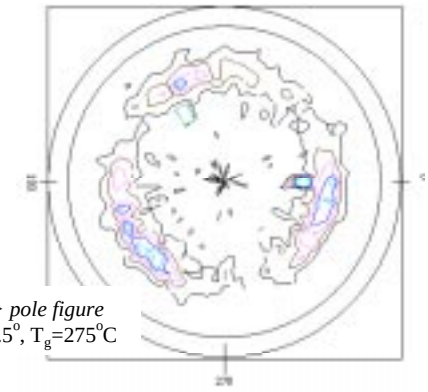

<200> pole figure
$2\theta = 34.5^{o}$, $T_g = 275^{o}C$

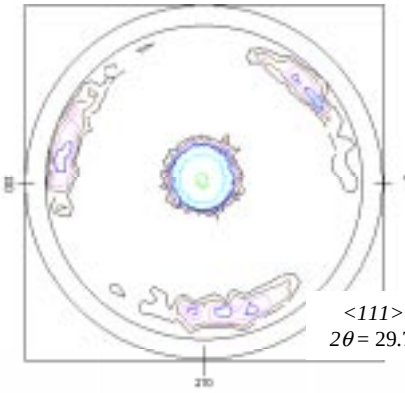

<111> pole figure
$2\theta = 29.7^{o}$, $T_g = 275^{o}C$

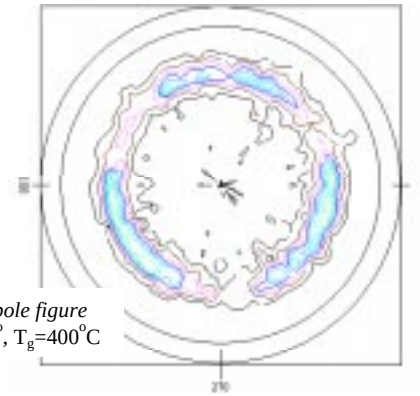

<200> pole figure
$2\theta = 34.5^{o}$, $T_g = 400^{o}C$

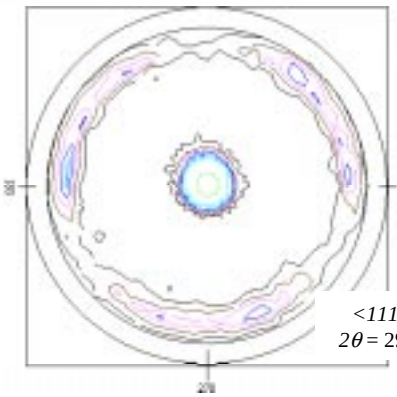

<111> pole figure
$2\theta = 29.7^{o}$, $T_g = 400^{o}C$

APPENDIX 1 (continued)

<200> and <111> x-ray pole figures taken from erbium hydride thin films grown onto Si(100) having a native oxide. This includes depositions at 30, 150 and 275°C.

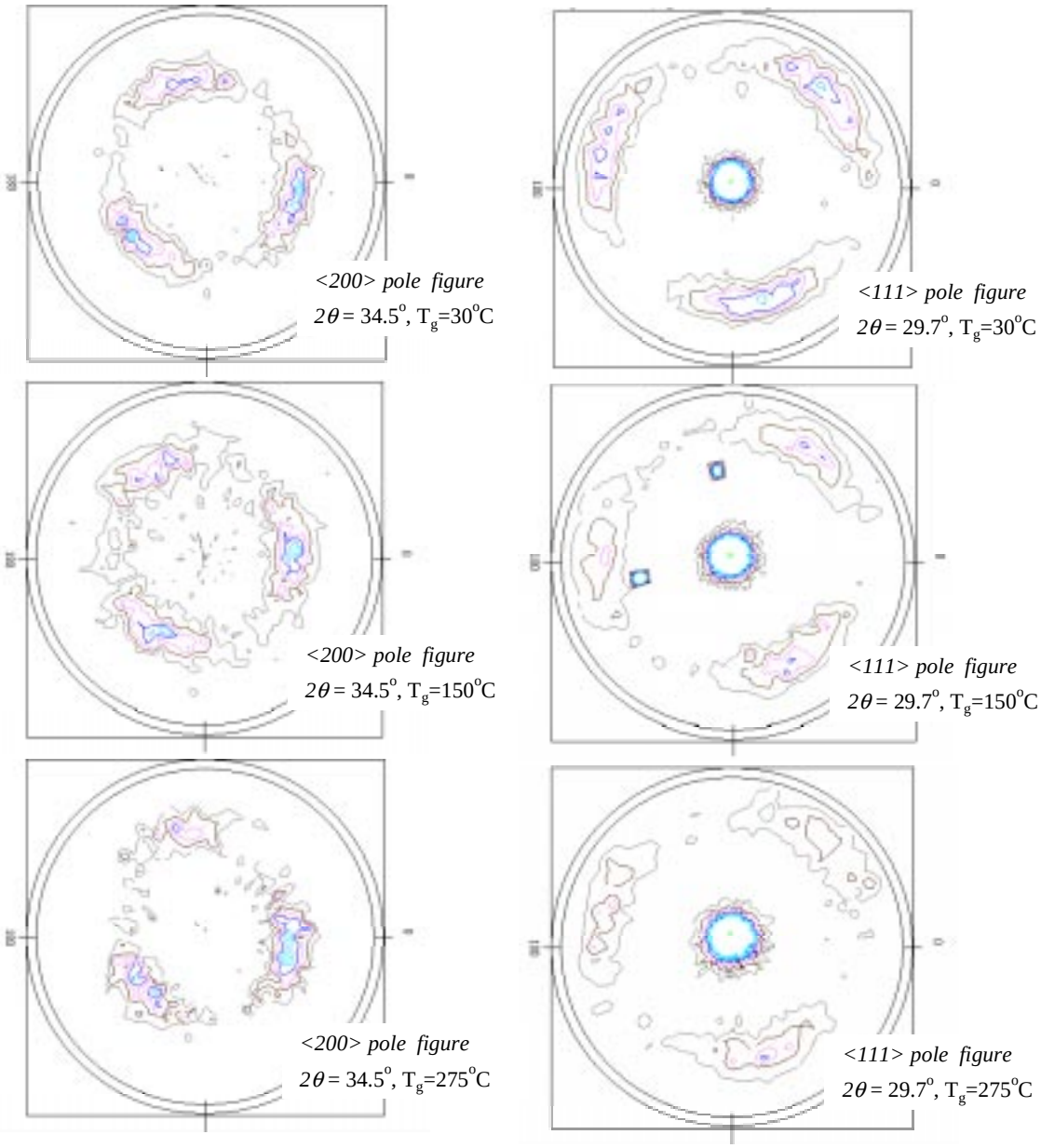

APPENDIX 2: Lattice reflections and associated lattice spacings for the cubic and hexagonal erbium hydride phases. Also listed are the values for the body centered cubic Er_2O_3 phase. These are taken from previous works.

Reflection	Lattice spacing
(111)	2.96 Å
(002)	2.57 Å
(220)	1.81 Å
(311)	1.54 Å
(222)	1.47 Å

Allowed reflections and lattice spacings for the cubic phase (typically having composition ErH_2)

Reflection	Lattice spacing
$(01\underline{1}0)$	3.13 Å
(0002)	3.26 Å
$(01\underline{1}1)$	2.82 Å
$(01\underline{1}2)$	2.26 Å
$(11\underline{2}0)$	1.81 Å

Allowed reflections and lattice spacings for hexagonal ErH_3 phase

Reflection	Lattice spacing
(110)	7.51 Å
(200)	5.30 Å
(211)	4.32 Å
(220)	3.74 Å
(310)	3.35 Å
(222)	3.05 Å
(321)	2.83 Å
(400)	2.65 Å
(411)	2.49 Å
(420)	2.37 Å
(422)	2.16 Å

Allowed reflections and lattice spacings for body centered cubic - Er_2O_3

APPENDIX 3: Transmission electron micrographs of ErH_3 film deposited onto Si(100) having a native oxide surface.

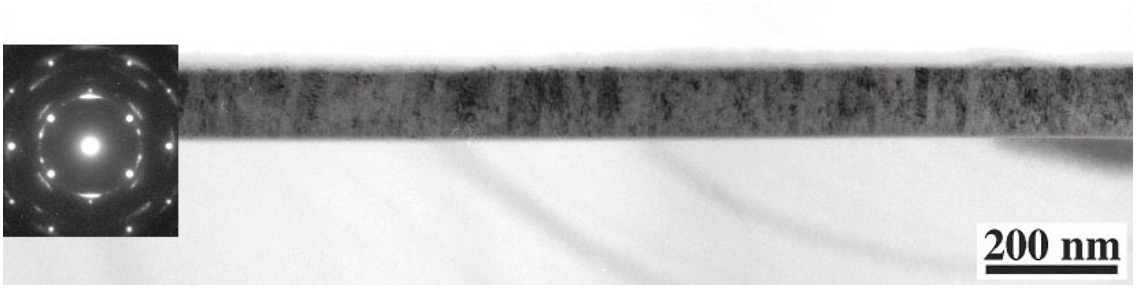

Cross section image of film and substrate. Growth temperature = 30°C.

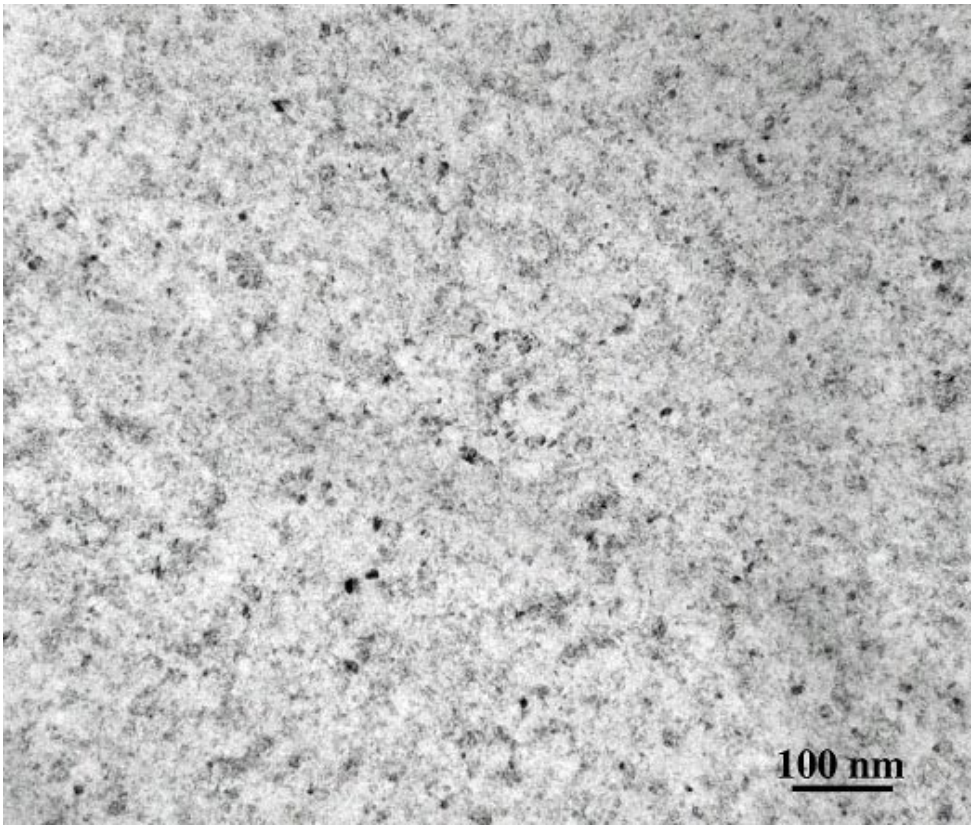

Plan view, dark-field, selected area aperature image of film grown at a temperature = 30°C.

APPENDIX 4: Procedure for calculating moduli of sapphire. Included are the c_{ij} for Al_2O_3 (from T. Goto et.al. J. Geophy. Res (1989)), the associated stiffness tensor (taken from J.F.Nye, *Physical Properties of Crystals*, Clarendon Press, Oxford, (1987)), calculated moduli in relevant directions, and schematic of crystallographic planes in alumina.

the c_{ij} for alumina are

c_{11} = 480 GPa along [100]
c_{33} = 490 GPa along [001]
c_{44} = 140 GPa transverse to [001]
c_{12} = 163 GPa
c_{13} = 116 GPa

$$\begin{pmatrix} c_{11} & c_{12} & c_{13} & 0 & 0 & 0 \\ c_{12} & c_{11} & c_{13} & 0 & 0 & 0 \\ c_{13} & c_{13} & c_{33} & 0 & 0 & 0 \\ 0 & 0 & 0 & c_{44} & 0 & 0 \\ 0 & 0 & 0 & 0 & c_{44} & 0 \\ 0 & 0 & 0 & 0 & 0 & 1/2(c_{11}-c_{12}) \end{pmatrix}$$

Using known c_{ij} for alumina and the stiffness tensor shown on the right we determine the relevant moduli as follows.

Apply biaxial condition, decompose in [11$\underline{2}$0]
Moduli for (0001) in [11$\underline{2}$0]: ***607*** **GPa**

Rotate tensor, apply biaxial condition, decompose in [0001]
(11$\underline{2}$0) in [0001]: ***551*** **GPa** (***522*** **GPa** in direction 90^o opposed)

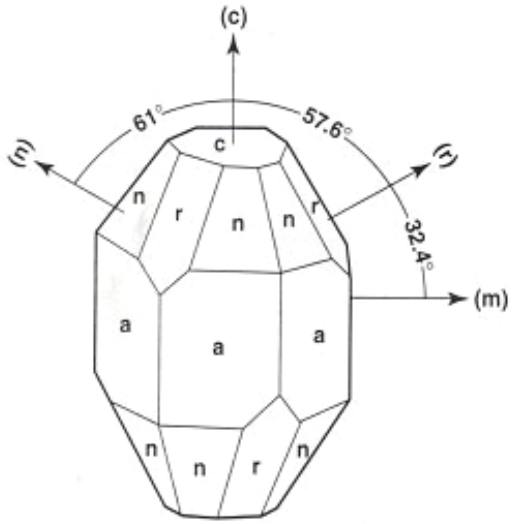

APPENDIX 5: Plots of stress-film thickness product versus film thickness for ion beam sputtered erbium hydride on Si(100) having a native oxide. Films develop a large compressive stress during deposition. Films maintain a compressive stress after cooldown from the growth temperature.

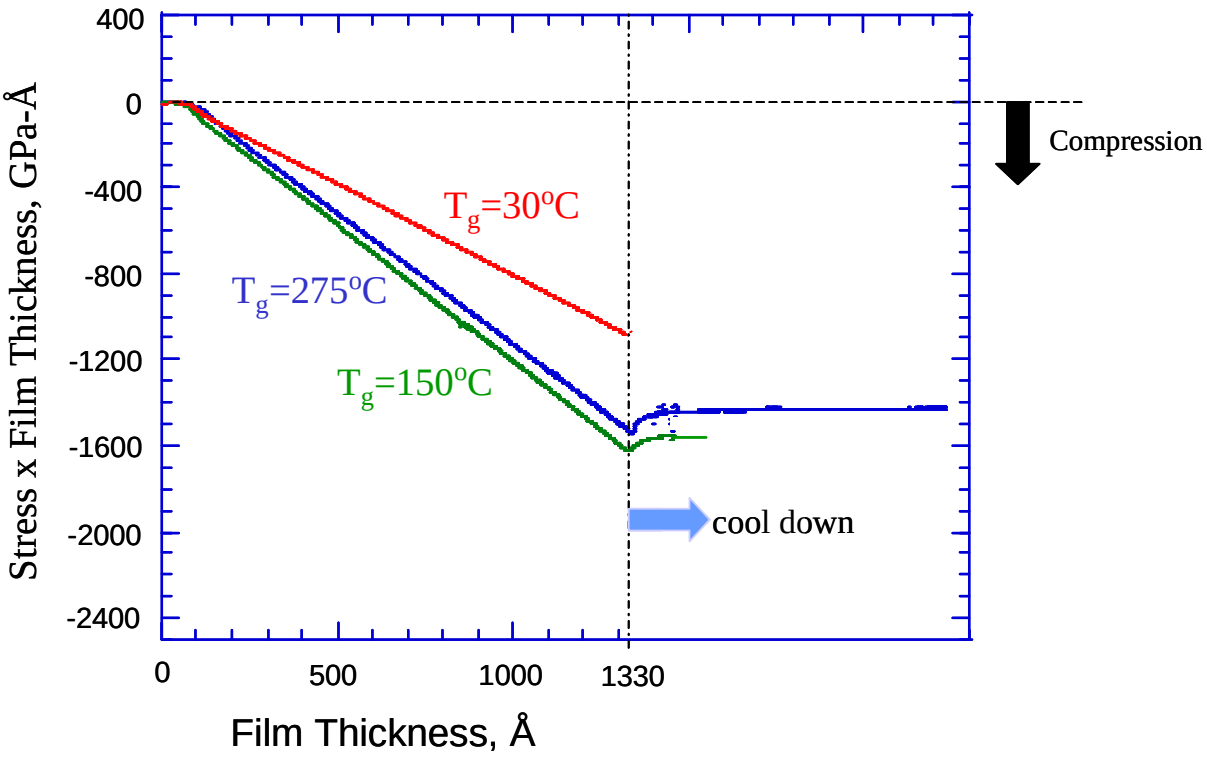

Evolution of stress during ion beam sputtering of erbium hydride thin films onto silicon substrates as determined by MOSS. A negative ordinate value represents a compressive stress.

APPENDIX 6: Plot of curvature changes developed during reactive deposition of scandium deuteride. Note, the ordinate limits in this plot are less than those shown in Figure 31. Again this demonstrates minimal changes in cermet wafer curvature (i.e., a low stress) during reactive deposition of a ~'1x' scandium deuteride film. Film composition is $ScD_{1.83}$.